Large-Scale Air Mass Characteristics Observed Over the Remote Tropical Pacific Ocean During March-April 1999: Results from PEM Tropics B Field Experiment

Edward V. Browell[1], Marta A. Fenn[2], Carolyn F. Butler[2], William B. Grant[1], Syed Ismail[1], Richard A. Ferrare[1], Susan A. Kooi[2], Vince G. Brackett[2], Marian B. Clayton[2], Melody A. Avery[1], John D. Barrick[1], Henry E. Fuelberg[3], Reginald E. Newell[4], Yong Zhu[4], and M. J. Mahoney[5]

[1]NASA Langley Research Center, MS-401A, Hampton, VA 23681

[2]Science Application International Corporation, Hampton, VA 23666

[3]Florida State University, Tallahassee, FL

[4]Massachusetts Institute of Technology, Cambridge, MA

[5]California Institute of Technology, Jet Propulsion Laboratory, Pasadena, CA

Draft PEM Tropics B Manuscript

May 15, 2000

Abstract

Eighteen long-range flights over the Pacific Ocean from 38°S to 20°N and 166°E to 90°W were made during the NASA Pacific Exploratory Mission B (PEM Tropics B) conducted from March 6 to April 18, 1999. Airborne lidar systems were operated from the NASA DC-8 aircraft to remotely measure vertical profiles of ozone (O_3), water vapor (H_2O), aerosols, and clouds from near the surface to the upper troposphere along the aircraft flight track, and in situ measurements of O_3 and H_2O were also made on the DC-8 to complement the lidar remote measurements. The transition from northeasterly flow of Northern Hemispheric (NH) air on the northern side of the Intertropical Convergence Zone (ITCZ) to general easterly flow of Southern Hemispheric (SH) air south of the ITCZ was accompanied by a significant decrease in O_3 and aerosols and an increase in H_2O. Trajectory analyses indicate that the air north of the ITCZ came from Asia and/or the United States, while the air south of the ITCZ had a long residence time over the Pacific, and it probably originated in South America many weeks before. The air to the south of the South Pacific Convergence Zone (SPCZ) came rapidly from the west with an origin in Australia or Africa, and it had enhanced O_3 and aerosols and a decrease in H_2O associated with it. Average latitudinal and longitudinal O_3 and H_2O distributions were constructed from the remote and in situ O_3 and H_2O data, and these distributions are compared with the results from PEM Tropics A conducted in August-October 1996. Low O_3 was found throughout the troposphere across the entire Pacific Basin at low latitudes during PEM Tropics B. This was in strong contrast to the enhanced O_3 levels that were found across the central and eastern Pacific low latitudes during PEM Tropics A. Nine air mass types were identified for PEM Tropics B based on their O_3, aerosols, clouds and potential vorticity (PV) characteristics. The data from

each flight was categorized as to the identified air masses, and these results were binned with altitude in the seven regions. The NH air in the central and eastern Pacific had significantly different properties than the SH air south of the ITCZ. The NH was dominated by O_3 enhanced air from Asia or North America while the SH air between the ITCZ and SPCZ was characterized by reference or background air which had relatively low O_3 associated with it (<30 ppbv). The air south of the SPCZ was influenced by stratospheric intrusions and by the subsequent mixing of this air with tropospheric air to produce the enhanced O_3 levels found in these air masses. The average O_3 distributions, O_3 and H_2O correlations, and average air mass compositions observed over the Pacific are discusses in this paper, and they are compared to the results from PEM Tropics A.

1. Introduction

The NASA Pacific Exploratory Mission B (PEM Tropics B) was conducted from 6 March to 17 April 1999 to investigate the chemistry of the remote tropical Pacific during the early austral fall. This was the second in the series of NASA field experiments conducted in this region with the first one conducted from 30 August to 5 October 1996 (PEM Tropics A) [Hoell et al., 1999]. During PEM Tropics B, the NASA Langley airborne UV DIAL (Differential Absorption Lidar) and LASE (Lidar Atmospheric Sensing Experiment) systems were both operated from the NASA DC-8 aircraft in nadir and zenith modes to simultaneously measure vertical profiles of O_3, H_2O, aerosols, and clouds from near the surface to the upper troposphere along the aircraft flight track. In situ measurements of O_3 and H_2O were also made on the DC-8 that augment the lidar remote measurements. The flight tracks of the DC-8 during PEM Tropics B are shown in Figure 1. A

discussion of the PEM Tropics B science objectives and the characteristics of the instrumentation on the DC-8 and P-3 aircraft are given in the overview paper by Jacob/Davis et al. [2000].

Eighteen DC-8 flights were made during the PEM Tropics B field experiment from bases in Hawaii, Fiji, Tahiti, and Easter Island. Local flights were performed from these locations, and long-range survey flights were conducted between the bases and on the way from the NASA Dryden Flight Research Center at Edwards Air Force Base, California, to Hawaii and on return to Dryden from Easter Island with a stop in Costa Rica. Details of the flight objectives and the specifics of each flight are given in the overview paper [Jacob/Davis et al., 2000]. The survey flights of the DC-8 consisted mainly of en route ascents and descents with short, typically less than 20 minute, constant altitude legs at specific altitudes of interest identified using the remote real-time lidar data. This allowed for extensive vertical sampling of the troposphere along the flight track. On local flights, the general strategy was to survey the troposphere along the flight track with the lidars, and to select the geographic region and altitudes of most interest for comprehensive in situ sampling. This approach allowed for the real-time synergistic use of data from the various sensors on the DC-8 to maximize the efficiency of the sampling strategy.

This paper briefly reviews the characteristics of the UV DIAL and LASE systems, discusses the results from the PEM Tropics B mission, and compares these results with the PEM Tropics A mission conducted during the biomass burning season over this same region.

2. Instrumentation and Methodology

The current airborne UV DIAL system has been described in detail in several recent publications [Richter et al., 1997, and Browell et al., 1998]. In this system, two 30-Hz,

frequency-doubled Nd:YAG lasers are used to sequentially pump two high-conversion-efficiency tunable dye lasers that are frequency-doubled into the UV to produce the on-line (289 nm) and off-line (300 nm) wavelengths for DIAL O_3 measurements. The residual 1064-nm and 600-nm beams from the frequency-doubling process of the Nd:YAG and dye lasers, respectively, are transmitted along with the UV DIAL wavelengths. In total there are four wavelengths (289, 300, 600, and 1064 nm) transmitted simultaneously into the atmosphere below and above the aircraft for lidar measurements of O_3, aerosols, and clouds from near the surface to about 3 km above the tropopause. This system has been used extensively in airborne investigations of tropospheric and stratospheric processes over the last twenty years [see e.g., Browell, 1983, 1989; Browell et al., 1998], including several NASA Global Tropospheric Experiments over the Pacific. These included PEM West (Pacific Exploratory Mission-West) field experiments in the late summer of 1991 (PEM West A) [Browell et al., 1996a] and late winter of 1994 (PEM West B) [Fenn et al., 1996] and the first PEM Tropics field experiment conducted in the late summer of 1996 [Fenn et al., 1999]. This system has an absolute measurement accuracy for O_3 measurements of better than 10% or 2 ppbv (parts per billion by volume) with a vertical resolution of 300 m and an averaging time of 5 minutes or about 70-km horizontal resolution at DC-8 ground speeds and a measurement precision of 5% or 1 ppbv [Browell, 1983; Browell et al., 1983, 1985]. Intercomparisons between in situ and UV DIAL O_3 measurements are made throughout the course of a field experiment to insure the accuracy of the measurements is being maintained [see e.g., Fenn et al., 1999].

The LASE system was initially designed for and operated from the NASA high-altitude ER-2 aircraft [Browell and Ismail, 1995; Moore et al., 1997; Browell et al., 1997]. This system uses a Ti:sapphire laser that is pumped by a double-pulsed, frequency-doubled Nd:YAG to produce

laser pulses in the 815-nm absorption band of H_2O. The wavelength of the Ti:sapphire laser is controlled by injection seeding with a diode laser that is frequency locked to a H_2O line using an absorption cell, and each pulse pair consists of an on-line and off-line wavelength for the H_2O DIAL measurements. The LASE system was operated for the first time from the NASA DC-8 in the 1998 Convection and Moisture Experiment (CAMEX-3) [Ferrare et al., 1999; Browell et al., 2000], and during this experiment, LASE was configured to simultaneously measure H_2O, aerosol, and clouds below and above the DC-8 using a back-to-back transmitter-receiver arrangement similar to that used for the UV DIAL system. This enabled LASE measurements to be made from near the surface into the upper troposphere.

The accuracy of the LASE H_2O profile measurements was shown to be better than 6% or 0.01 g/kg, whichever is greater, in a major validation experiment conducted in 1995 involving two other aircraft (C-130 and Lear jet) instrumented with several in situ H_2O sensors on each and one with a H_2O DIAL system; radiosonde balloons; and a ground-based Raman lidar [Browell et al., 1997]. Additional intercomparisons were conducted during the TARFOX (Tropospheric Aerosol Radiative Forcing Experiment) field experiment conducted in 1996 [Ferrare et al., 2000a,b]. Once the LASE system was configured for operation from the DC-8 in the simultaneous nadir and zenith mode of operation, additional comparisons were made with other sensors to insure the accuracy of the H_2O measurements. Ferrare et al. [1999] and Browell et al. [2000] discuss these intercomparisons in the context of the CAMEX-3 (Convection And Moisture Experiment-3) field experiment conducted in 1998 to study hurricane characteristics with a large ensemble of airborne instruments. The results were consistent with the initial LASE validation experiments.

An example of comparisons between LASE nadir and zenith H_2O profile measurements and the in situ H_2O measurements from three different H_2O sensors on the DC-8 and a locally launched radiosonde is shown in Plate 1. The sampling between the various sensors is very different, and yet there is good agreement between most of the measurements with the chilled hygrometer having the greatest disagreement at H_2O levels below 2 g/kg, where it is expected to be the least accurate. The radiosonde launched from Tahiti generally agrees with the other measurements with the largest deviation in the mid troposphere of ~0.15 g/kg. The cryogenic and diode laser hygrometer measurements were smoothed to the same 500 m vertical resolution of the LASE measurements, and they showed excellent agreement with each other and with the LASE measurements. This further demonstrates the measurement capability of the LASE across a wide range of H_2O concentrations.

Since the UV DIAL remote O_3 profiles start about 750 m above and below the aircraft, the ozone distribution across this region is estimated by interpolating between the nadir and zenith UV DIAL measurements with the in situ O_3 measurement used to constrain the interpolation in the middle. Ozone distributions were also extrapolated from the lowest UV DIAL measurement altitude (usually below 1 km) to the surface using the gradient in ozone concentrations determined from the in situ measurements. These techniques were previously discussed for the UV DIAL O_3 distributions in the PEM Tropics A field experiment [Fenn et al. [1999]. An example of the resulting O_3 distribution is shown in Plate 2 for the flight from NASA Dryden to Hawaii (Flight 5). The aerosol scattering ratio distribution derived from the UV DIAL measurements on the same flight is also shown in Plate 2. The aerosol scattering ratio is the ratio of the amount of backscattered laser light from aerosols alone to the amount of backscattered laser light that would be expected from a clean (aerosol free) molecular atmosphere. The relative

IR (1064 nm) lidar backscatter distribution, which represents scattering from aerosols and molecules, is normalized to a region that is estimated to be clean (molecular scattering only), and this results in the total atmospheric scattering ratio. In this calculation, the relative molecular backscattering distribution is determined from the remote atmospheric pressure and temperature measurements of the JPL Microwave Temperature Profiler (MTP) along the flight track or from a meteorological analysis if the MTP data are not available. The aerosol scattering ratio is then just the total atmospheric scattering ratio minus one. Note that there is no attempt to correct for aerosol and cloud attenuation in these distributions.

Ten-day back trajectories for air parcels at 500 mb along the flight track are also shown in Plat 2. These back trajectories were conducted using the Florida State University (FSU) kinematic back trajectory model. Air parcels along the flight track are selected at specific pressure altitudes, and these air parcels are followed back to their origin ten days earlier (unless the trajectory terminates early at the surface). The consistency of the trajectories can be tested by using an ensemble of air parcels. This is discussed in detail by Fuelberg et al [2000]. The back trajectories shown in this paper are used to represent the general air mass characteristics that are represented by the source region of the air.

3. Results and Discussion

3.1 Air Masses Observed Over Pacific

A major air mass transition was observed on the survey flight from California to Hawaii on 6 March 1999 (Flight 5). Plate 2 shows the O_3 and aerosol distributions observed along the flight track and the ten-day back trajectories ending at the 500 mb level along the flight track. The air

off the coast of California had significant levels of O_3 and enhanced aerosol loading across the entire troposphere, and this situation gradually changed on the southwest flight leg to where the enhanced aerosol loading was no longer present and where O_3 levels in the low 20 ppbv level were observed near the surface. Cirrus clouds were seen with tops to as high as 12 km which was just under the tropopause. A stratospheric intrusion was observed on the west-bound leg with ozone values over 60 ppbv extending down to 8 km at 20°N. This intrusion modified the O_3 levels in the mid troposphere while the levels below 2 km were in the 20-40 ppbv range. The ten-day back trajectory analysis for air parcels with end points at 500 mb shows that the origin of the air closest to the California coast probably came from Asia. Along the track the origin of the air changed to coming from the southwest and then the west with less aerosols and O_3 associated with it. This was a clear transition from a continental source to more of a marine background condition with the additional influence of the stratospheric intrusion.

There was a large contrast found in the characteristics of air masses in the northern hemisphere(NH) and southern hemisphere (SH). As described by Fuelberg et al. [2000], the convergence of NH air and SH air at low altitudes occurs in a region called the Intertropical Convergence Zone (ITCZ), and at the time of PEM Tropics B, the ITCZ is located north of the equator between about 3-10°N. Plate 3 shows the O_3, H_2O, and aerosol distributions across the ITCZ on the flight from Hawaii to Fiji on 17-18 March 1999 (Flight 9). The transition from NH air to SH air can be seen in the abrupt decrease in O_3 levels from 20-30 ppbv near the surface and 40-60 ppbv in the mid troposphere to less than 10 ppbv near the surface and 20-40 ppbv in the free troposphere. This decrease in O_3 was anticorrelated with the change in H20 which generally increased everywhere below about 7 km. A convective outflow from upwind cloud activity can be readily seen in the H_2O data between 2130 and 2230 UT at an altitude of 6.5 km. The depth

of the marine boundary layer also increased into the SH air. There is some evidence for there being a slight enhancement in aerosols in the NH air (see aerosol layer at ~4 km near 2130 UT). Cirrus clouds can be seen under the tropopause, and the height of the tropopause increased along the flight track from ~13 km in the NH to over 15 km south of the equator. A series of trajectories at three end point pressure levels (850, 500, 200 mb) are given in Plate 4 along this flight track. In the middle and lower troposphere north of about 10°N , the flow of the NH air was predominantly from Asia, while the flow to the south was entirely easterly near the surface and variable in the mid troposphere with light winds a long residence times over the Pacific. In the NH upper troposphere the flow was organized with a strong flow from the west, while the SH flow was light and without organization . This is reflected in the vertical homogeneity of the SH air with low O_3 and elevated H_2O throughout the troposphere.

The second major transition between air masses occurs across the South Pacific Convergence Zone (SPCZ) [Fuelberg et al., 2000]. The atmospheric cross sections from the Fiji local flight on 20 March 1999 (Flight 10) show the differences across this region (Plate 5). The flight initially starts out south of the SPCZ and crosses the SPCZ twice at about 0000 and 0350 UT. Ozone decreased by over a factor of two from south to north of the SPCZ, and H_2O was again anticorrelated with O_3. Thin cirrus clouds were ubiquitous to the north of the SPCZ, and there is an indication of a change in boundary layer aerosol scattering characteristics in this region. Relative humidity (RH) was calculated from the LASE H_2O and MTP temperature measurements, and the change in RH across the SPCZ is much greater than the H_2O change. The large RH levels throughout the troposphere correlates with the low O_3 across the region, and modeling studies have shown [Crawford et al., 2000] that O_3 loss is expected to dominate at all altitudes under these conditions. The back trajectory analysis for this case is shown in Plate 6.

North of about 20°S the air masses are generally coming from the east at all altitudes with long residence times over the Pacific. South of 20°S, the air is mainly from the west with light winds at the surface and stronger winds out of the west at higher altitudes. This change in nature of the air masses across the SPCZ results in a marked difference in the chemistry and meteorological parameters associated with each region. This is very similar to the change in conditions across the ITCZ with the air south of the SPCZ having more of a continental influence than the tropical Pacific air north of the SPCZ. An additional example of the transition across the SPCZ was obtained on 31 March on a local flight from Tahiti (Flight 14). The H_2O and O_3 distributions observed across the SPCZ are shown in Plate 7. The dryer air with enhanced O_3 to the south of the SPCZ can be seen in contrast to the more moist air with lower O_3 to the north of this convergence region. The increase in H_2O was nearly an order of magnitude near the surface while O_3 decreased more than a factor of three below 6 km. This further indicates the degree of difference that can exist in the chemistry and composition of the two air masses.

Another factor that contributes to determining the composition of the southern mid latitude air comes from stratospheric intrusions. The clearest example of this was found on 10-11 April 1999 on a local flight southwest of Tahiti (Flight 18). The O_3, H_2O, RH, and aerosol/cloud observation on that entire flight are presented in Plate 8. Also shown on each color plot are the isopleths of potential vorticity (PV) derived from ECMWF (European Center for Medium-range Weather Forecasting) analyses along the flight track. The PV analyses agree well with the general O_3 features observed in the intrusion even though the PV analyses do not have the spatial resolution of the lidar data. The PV analyses indicate that there should be enhancements of 8-16 ppbv in O_3 from the stratosphere even down to near the surface assuming a relative factor of about 4 ppbv/PV units in the lower stratosphere, and there is some indication that the O_3

distribution in the lower troposphere is enhanced by the intrusion to varying degrees. This is not to ascribe all of the variation to this or another up wind intrusion, however, there is reason to attribute some of the O_3 enhancement to a stratospheric source. We will address this later in this paper. The cirrus clouds are on the equatorward side of the intrusion, and their tops go up to the local tropopause altitude. The H_2O distribution shows a more moist troposphere on the north side of the intrusion and a generally drier atmosphere near the intrusion. The RH distribution shows the location of the intrusion even better than the H_2O distribution. The low RH conditions (<10%) associated with the intrusion is much lower than the moderate (>40%) to high (>70%) RH levels seen outside the intrusion with high RH levels even near the tropopause in vicinity of the cirrus clouds.

The final flight of PEM Tropic B from Costa Rica to California provided an opportunity to observe a range of air mass characteristics from a clean tropical marine air mass to a continental air mass with a combination of aerosol and pollution sources. Plate 9 shows the O_3, aerosol, H_2O, and RH distributions for Flight 22 on 18 April 1999. South of about 13°N, the distribution of these parameters showed a tropical marine environment which is very moist, with low O_3 in the boundary layer and lower troposphere, and low aerosol loading in the free troposphere. There is a transition in atmospheric conditions in the mid and lower troposphere between 13 and 22°N. Ozone generally increases along this leg north of 13°N, and the aerosol loading also increases up to a depth of 10 km near 34°N. The H_2O gradually decreases across this region, and the RH shows the greatest change going from near saturation conditions in the tropical marine air to very dry conditions (<10%) in the air which has considerable aerosol loading in it. Cirrus clouds were observed on the middle of this flight with bases as low as 10 km and tops as high as 15 km. Plate 10 shows a vertically expanded view of the aerosol scattering ratio, aerosol

depolarization, and RH distributions on the northern end of this flight. The aerosol depolarization at 578 nm was measured using simultaneous detection of the parallel and perpendicular components backscattered from the atmosphere, and the total depolarization ratio is the ratio of the perpendicular to parallel lidar returns. The aerosol depolarization contribution to the total atmospheric depolarization, which includes both the depolarization from aerosols and molecules (~1.5% from molecules alone), is estimated using the aerosol scattering ratio at this wavelength. The air with the heavy aerosol loading and the very low RH values, starting near the surface near 22°N and extending up to about 4 km near 30°N, exhibits aerosol depolarization levels above 25% with some exceeding 40%. The wavelength dependence of lidar backscattering between 578 and 1064 nm was found to be very low (<0.5). These two factors indicate that the aerosols in this region are probably large desert aerosols. Because of their size and concentration, this was thought to come from a continental source within a few days upwind. Ten-day back trajectories at three level are shown in Plate 11 for this flight. The low altitude trajectories at 850 mb show that at the southern end of the flight leg the air came across Central America from the tropical Atlantic Ocean while the air in the transition region came from the Caribbean. North of about 24°N, the air came south along a long fetch across the desert regions of southwestern U.S. and northwestern Mexico. At 500 mb the source of the air was similar to that at lower altitudes along the flight track to 17°N where the air flow changed direction and the air then came from the tropical Pacific. North of 28.5°N, the flow was strong from the west with a source from somewhere over Asia. The upper altitude flow was similar to that at 500 mb, but the flow on the southern end of the leg was now more from the tropical Pacific. This is an excellent example of how extreme variations in air mass sources contribute to determining the composition and chemistry of the atmosphere along a cross section of the atmosphere. The

following sections discuss the average composition and general air mass characteristics of the atmosphere investigated during PEM Tropics B.

3.2 Average Ozone and Water Vapor Distributions and Correlations

Average latitudinal and longitudinal O_3 cross sections were produced from average O_3 cross sections from each flight which included the interpolation and extrapolation of the O_3 profiles constrained by the in situ measurements and the averaging of the data to produce a single O_3 profile in a 0.25°-latitude or 0.50°-longitude bin for each flight. The individual flights were weighted equally in determining the average O_3 profile for each bin [Browell et al., 1996b]. Plate 12 shows the average latitudinal and longitudinal O_3 cross section obtained for PEM Tropic A and B. The ranges of the averages were chosen to obtain a latitudinal cross section representative of the central Pacific (170°W to 120°W) and a longitudinal cross section representative of the southern tropical Pacific (30°S to 0°N).

The differences in the large-scale O_3 distribution between PEM Tropics A and B is clearly evident in Plate 12. The extensive burning in Africa, South America, and many other regions during the austral winter contribute to the increased photochemical O_3 production that was observed downwind over the remote central Pacific during PEM Tropics A [Talbot et al., 1999; Schultz et al., 1999; Fuelberg et al., 1999; Fenn et al., 1999; Singh et al., 2000]. In PEM Tropics A the SPCZ was closer to the ITCZ and it did not extend as far southeast as it did in PEM Tropics B, and as a result this allowed for more of a westerly flow of biomass burning products and enhanced O_3 across the Pacific. The enhanced O_3 from biomass burning can be seen throughout the troposphere to the south of 10°S, and this extends to the north to nearly the ITCZ

at about 9°N. Enhanced O_3 levels in the NH air to the north of the ITCZ can be seen in the figure. The region of very low O_3 (<20 ppbv) was from 6°S to 18°N near the surface, and low O_3 was also found in the upper troposphere due to convection principally coming from the ITCZ. The longitudinal O_3 distribution during PEM Tropics A shows the general transport of the biomass burning plumes to low latitudes in the central Pacific while the region of very low O_3 was the most extensive in the western Pacific. Transport of biomass burning plumes across the Pacific in the westerlies is also indicated in the enhanced O_3 distribution in the mid troposphere in the eastern Pacific.

The latitudinal O_3 distribution from PEM Tropics B clearly shows the average location of the ITCZ and SPCZ across the central Pacific. The enhanced O_3 throughout the troposphere in the NH air north of the ITCZ at about 12°N is in contrast to the low O_3 throughout the troposphere in the SH air from there to the SPCZ at about 22°S. The air to the south of the SPCZ was enhanced in O_3 from continental sources and stratospheric intrusions. The longitudinal distribution shows the largest region of very low O_3 in the western Pacific, but unlike PEM Tropics A, the very low O_3 region extended across the entire Pacific at low altitudes. Ozone was low (<30 ppbv) across the entire region from the surface to the tropopause which decreased in altitude to the east from 15 to 12 km.

The average latitudinal and longitudinal H_2O distributions were constructed from the remote LASE measurements using the same techniques as was used for the O_3 distributions. The H_2O distributions for PEM Tropics B are shown in Plate 13. The change in H_2O across the ITCZ at about 12°N can be seen in the decrease in altitude of the 1 g/kg level from about 7 to 4 km. Water vapor levels in the marine boundary layer were significantly lower north of the ITCZ. The SPCZ is much more difficult to see in the average H_2O distribution, but the transition covers

the region from 18 to 24°S. The change in H_2O to the east across the Pacific shows a general drying of the troposphere at all altitudes with the largest changes being below 4 km.

Composite average profiles for H_2O and O_3 were calculated for the NH air north of 15°N, the SH tropical Pacific air between 10°N and 20°S, and the SH subtropical air south of 25°S, and they are presented in Plate 14. The average value, the $\pm 2\sigma$ standard error of the average, and the $\pm 1\sigma$ standard deviation of the measurements are shown in each altitude interval. The H_2O is considerably higher in the SH tropical Pacific, particularly in the mid to upper troposphere. There is no statistical difference in our observed H_2O profiles for the NH air and SH subtropical air above 2 km. Near the surface the SH subtropical air appears to be slightly drier than the NH air. The O_3 profile for the SH tropical Pacific was lower than the other two regions at all altitudes. This profile starts at 12 ppbv near 1 km and does not exceed 28 ppbv until above 11 km. The SH subtropical O_3 profile is less than 10 ppbv greater than the SH tropical Pacific O_3 profile up to about 8 km where the lower tropopause and stratospheric intrusions make a significant contribution at higher southerly latitudes. The NH O_3 profile shows a more significant O_3 enhancement throughout the mid to lower troposphere than either of the other profiles, and this difference was maintained compared to the SH tropical Pacific profile to above 11 km.

The H_2O to O_3 correlations were examined to better quantify the differences in the three regions, and these results are shown in Plate 15. There was not a statistical difference between the H_2O to O_3 correlations at H_2O levels greater than 1 g/kg which is predominantly from air below 5 km in the SH subtropics and below 7.5 km in the SH tropical Pacific. Above these altitudes, the correlation changed in the upper troposphere of the SH subtropics as this air became associated with more air with stratospheric influences. The H_2O to O_3 correlation was

distinctly different for the NH air which was driven by the very different air mass origins. This was true for all H_2O levels greater than 0.1 g/kg compared to SH tropical Pacific and greater than 1 g/kg compared to SH subtropics. From these results it appears that there is a clear delineation between the SH and NH air masses with respect to H_2O and O_3, but the distinction between the SH subtropical air south of the SPCZ and the SH tropical Pacific air is more difficult to make on average possibly due to the limited sampling of air in the former category or the variability in the location or strength in the SPCZ.

3.3 Air Mass Characterization

A general categorization of the air masses observed during PEM Tropics B was done by using a variation of the principal component analysis on the O_3 and aerosol distributions measured with the UV DIAL system and the potential vorticity (PV) information along our flight track derived from meteorological analyses from the European Center for Medium-range Forecasting (ECMWF). This approach was first used by Browell et al. [1996b] in an analysis of the air mass types over the tropical Atlantic Ocean during TRACE A, and it was recently used in the analysis of the PEM Tropics A air mass types [Fenn et al., 1999]. Since the background or reference air in the SH tropical Pacific during PEM Tropics B was so much different from what was present during PEM Tropics A, a different reference O_3 profile needed to by chosen as a discriminator. A reference O_3 profile was selected to be an approximation of the average in situ O_3 profile obtained between 10°S and 10°N. This average in situ O_3 profile and the selected O_3 discriminator is shown in Figure 2 along with the average in situ O_3 profile from 40 to 20°S. The average in situ profiles for these regions are very close to the O_3 profiles shown in Plate 14 for

the more extensive measurements combining the remote and in situ O_3 measurements. These profiles also compared well to the average O_3 profiles obtained from ozonesondes launched from Tahiti, Fiji, and Samoa during this field experiment, and thus for the purposes of air mass identification, the O_3 discriminator was assumed to be representative of the background or reference O_3 profile over the tropical Pacific during this experiment. The various air mass types are then judged against this reference O_3 profile with additional differentiation from an examination of the aerosol backscatter levels and PV amounts in these air masses. The air mass categories are basically the same as was used in our PEM Tropics A analysis [Fenn et al., 1999]. There are nine categories of air masses that were identified using this technique. The air mass types and their criteria are:

Reference (REF): Ozone values within 20% of reference profile (RP) and low IR aerosol scattering ratios (S<0.2).

Background Plume (BPLU): Same as REF except with enhanced aerosols (S>0.2).

Near Surface (NS): Air with high aerosol loading associated with boundary layer.

Clean Pacific (CP): Ozone more than 20% below RP and S<0.2.

Convective Outflow (CO): Same as CP except cirrus clouds are in the vicinity.

High Ozone Plume (HPLU): Ozone more than 20% above RP and S>0.2.

High Ozone* (HO3): Ozone more than 20% above RP, S<0.2, and amount of O_3 attributable to stratosphere is <25%.

High Ozone Mixture* (HO3M): Same as HO3 except the amount of O_3 attributable to stratosphere is 25-60%.

Stratospherically Influenced* (SINF): Same as HO3 except that the amount of O_3 attributable to stratosphere is >60%.

*Note that in the calculation of the amount of O_3 attributed to the stratospheric component it is assumed that the O_3 in the lower stratosphere has the following approximate relationship to PV: O_3 [ppbv] ~ 4.2 x |PV| [10^{-7} deg K m^2 kg^{-1} s^{-1}].

All of the UV DIAL observations were used to categorize the air masses for each flight by geographic location and altitude. An example of the air mass characterization done for the first half of Flight 18 on 10-11 April 1999 is presented in Plate 16. This is the same flight where the O_3, aerosols, H_2O, and RH were presented for it in Plate 8. In this case, which discussed previously in terms of the observed stratospheric intrusion, the air mass classification method identified a large portion of the air above 2 km as having a strong stratospheric influence (SINF). There are enhanced O_3 regions where the stratospheric component could only explain a moderate amount of the enhanced O_3 (HO3M), and a few small regions where there was very little stratospheric contribution (HO3). It is clear that the relatively low resolution PV analyses cannot be expected to map all the features that the DIAL system can observe, and thus there will be some unavoidable misrepresentation of air masses between these groups in the vicinity of highly structured intrusions. Also seen in this example is air associated with cloud convection with its associated low O_3 in the vicinity of cirrus clouds (CO), near surface air up to about 3 km (NS), and reference air (REF) predominantly on the equatorward side of the intrusion.

The results from each flight were grouped together into averages based on the regions identified in Figure 1. Several of the regions are the same as the regions used previously in the PEM Tropics A field experiment [Fenn et al., 1999]. This was done to permit more of a direct

comparison of the results between the field experiments. Plate 17 presents the results for all of the PEM Tropics B regions. The contrast in the air mass types identified in the NH (CPNH and EPNH) compared to the low latitude cases (CPLL and EPLL) is readily apparent. There is a significant amount of enhanced O_3 that is not attributed to stratospheric influence (HO3) in the NH, and in the NH eastern Pacific the amount of enhanced O_3 associated with enhanced aerosols increases significantly over the NH central Pacific. There is some contribution from the stratosphere in the mid to low troposphere over the NH central Pacific. At low latitudes over the central Pacific (CPLL) and eastern Pacific (EPLL), the situation is about the same with the background or reference air dominating the distribution below 10 km with some varying contributions (up to ~20%) from convective outflow of low O_3 air and enhanced O_3 from photochemical production (HO3) and from a mixture of photochemical production and some stratospheric influence (HO3M). In the western Pacific low latitudes (WPLL), the amount of convective outflow of low O_3 (CO) into the 3 to 13 km region is a major factor in determining the distribution of O_3 in the mid to upper troposphere. The mid latitude regions are very similar between the central Pacific (CPML) and the eastern Pacific (EPML), and the stratospherically influenced air (SINF) is contributing to the O_3 budget all the way down to the surface. While the SINF category was decreasing in frequency with altitude, the amount of HO3M was increasing to significant levels, which also indicates that there is still some stratospheric influence even though it is has been more mixed with tropospheric air.

The results from PEM Tropics A [Fenn et al., 1999] show a dominant influence of enhanced O_3 air masses (>60%) attributed to photochemical production (HPLU and HO3) at mid latitudes in the western and central Pacific (WPML and CPML). These air masses also had significant impact (>30%) in the mid troposphere even at low latitudes. Convective outflow of low O_3 air

from the surface to 7 to 15 km was frequently observed in the central Pacific low latitude case during PEM Tropics A, but in PEM Tropics B, this was not observed to occur as often. This might be due to the smaller contrast in O_3 distribution between the surface and the upper troposphere and an O_3 discriminator that possibly made it more difficult to detect this type of air mass.

The average composition for the air masses south of the ITCZ is presented in Plate 18 along with the average O_3 profile for each air mass type. The reference air mass type occurred 44-53% of the time from 3 to 10 km and the average O_3 profile for it was very close to the discriminator O_3 profile. This provided added support for this air mass type being the principal component in this analysis. The balance of the air mass types in this region were mostly distributed between convective outflow (CO), high O_3 (HO3), and high O_3 mixed (HO3M) with CO more prevalent in the upper altitudes and HO3 and HO3M more frequently observed in the lower free troposphere. As was expected, the near surface air dominated the air mass types below 3 km, and in the upper troposphere the frequency of observations of stratospherically influenced air (SINF) increased with altitude to the average tropopause level above 16 km where it was more than 86% of the time. There were few observations of air in the categories of aerosol plumes with background levels of O_3 (BPLU) or very low O_3 air in free troposphere not associated with convective outflow (previously called "clean Pacific" air, CP). The average O_3 profiles for the various air mass types shows that at the lowest altitudes in the free troposphere (~1-3 km) the SINF and HO3M categories have the highest average O_3 levels associated with them, while above about 7 km, the SINF category has the highest observed O_3 levels. The HO3 and HO3M categories have similar O_3 profiles above 6 km , while below 6 km, HO3 is comparable to HPLU

and NS at even lower altitudes. The CO O_3 profile was constant at about 17 ppbv from about 5 to 13 km, and CP O_3 profile was similar to CO with it decreasing to 5 ppbv at 1 km.

The average PV profiles for each air mass type is also shown in Plate 18, and SINF had the most PV of all above 6.5 km with HO3M having slightly more than SINF below that altitude. All of the other main categories of air mass types (REF, CO, and HO3) had generally PV$\leq$2 except for the REF profile above 9 km where it increased to PV~5 at 14 km. The explanation for this increase could be that the reference air in the upper troposphere could be a mixture of low O_3 air from an up wind convective outflow with some stratospheric air that would bring the average O_3 within the limits of the reference air O_3 discriminator. For example, a mixing of five parts of convective outflow air with O_3=17 ppbv and PV=2 with one part of stratospheric air with O_3=105 ppbv and PV=25 would produce air falling into the reference air category with O_3=28 ppbv and PV=4.9. Using PV as a discriminator might provide insight into this mixing process, but since PV does not have the resolution as the O_3 and aerosol measurements and the ECMWF analysis is based on sparse measurements across the south Pacific, this approach would be subject to even more uncertainties than the current method.

5. Summary and Conclusions

The PEM Tropics B field experiment provided the first large-scale characterization of air masses over the remote Pacific Ocean during the austral late summer to early fall. The simultaneous measurements of O_3, H_2O, aerosols, and clouds across the troposphere along the flight track of the DC-8 aircraft allowed for the more complete investigation of the remote troposphere over the Pacific than had been done before. This field experiment was conducted

during a time of low biomass burning in the SH, and these results provide an important contrast to the results of PEM Tropics A which was conducted in the austral late winter to early spring when biomass burning was widespread in the SH. In PEM Tropics B there was considerably less O_3 than was observed during the biomass burning period of PEM Tropics A. The air mass characterization for PEM Tropics A showed a large incidence in the HO3 category (>60%) in the lower troposphere of central Pacific low latitudes compared to less than 24% in PEM Tropics B. This was a direct result of long-range transport of photochemically produced O_3 from Africa and possibly as far away as Brazil.

The low O_3 observed in PEM Tropics B was primarily confined to the region between the ITCZ to the north and the SPCZ to the south, and this was associated with an easterly air flow across the Pacific of very moist air that progressively experience chemical O_3 loss into the western Pacific where the O_3 levels were found to be the lowest throughout the troposphere from <10 ppbv near the surface to <20 ppbv at 12 km. The O_3 was negatively correlated with H_2O across this region and when compared to the NH air to the north of the ITCZ which had higher O_3 but lower H_2O than the tropical Pacific air to the south. The NH air also had more cases of enhanced aerosols in plumes in the free troposphere than did the tropical Pacific air. The contrast in O_3, H_2O, and aerosols these air masses was seen on all flights that crossed the ITCZ. Much like the NH air to the north of the ITCZ, the SH air to the south of the SPCZ had higher O_3 and generally lower H_2O than the tropical Pacific air north of the SPCZ. The Asian/North American origins of the NH air and the Australian/African origins of the SH air are in contrast to the relatively slow easterly flow of tropical Pacific air that has not had continental influences from South America/Central America for many weeks. In the tropical Pacific air, the conditions are there for photochemical loss of O_3 (no continental pollution sources, high H_2O, and high

solar insolation), and this is what was observed with an average profile of O_3 in the region from 12 ppbv at 1 km to ~28 ppbv at 7 km and then relatively constant to above 11 km.

Since there was no SPCZ during the season of PEM Tropics A and there was extensive biomass burning that was taking place in Africa and other countries up wind of the south Pacific, the resulting influence of continental sources on the remote tropical Pacific was much greater than during PEM Tropics B. The blocking of the westerly flow due to the SPCZ enables the south Pacific to have a much larger influence of the easterly flow in the tropical Pacific. A comparison of the average latitudinal and longitudinal O_3 distributions for PEM Tropics A and B provides clear evidence of the differences in the flow conditions and chemistry between the two seasons. The latitudinal and longitudinal variations of the tropopause level can also be seen in the O_3 distributions for the two missions. Stratospheric intrusions were observed during both seasons with contributions to low latitudes (~20°S) in some cases. The average of the observed intrusions also contributes to the latitudinal structure of the tropopause and O_3 in the upper troposphere in the subtropics to mid latitudes.

Air mass characteristics were determined for seven regions over the Pacific. Nine air mass types were identified for PEM Tropics B based on their O_3, aerosols, clouds and PV characteristics. The data from each flight was categorized as to the identified air masses, and these results were binned with altitude in the seven regions. The NH air in the central and eastern Pacific had significantly different properties than the SH air south of the ITCZ. The majority of the air masses in the NH were associated with O_3 enhanced air in aerosol plumes or in low aerosol air not associated with stratospheric intrusions. This is consistent with the ten-day back trajectories that go back to Asia. The low latitudes across the Pacific have mostly low O_3 levels associated with the reference or background air and even lower O_3 associated with

convective outflow and very low "clean Pacific" air. At mid latitudes the stratospheric influence becomes stronger with intrusions and the subsequent mixing of stratospheric and tropospheric air in various proportions. The altitude dependence of this observed process was also determined. The average composition for the SH air south the ITCZ was found to be dominated across the mid troposphere by the reference air (45-50%) which has a low O_3 profile ($\leq$28 ppbv) to 15 km. Convective outflow of very low O_3 air from the surface, air with enhanced O_3 due to photochemistry, and air with enhanced O_3 due to a combination of photochemistry and stratospheric influences were found to be in comparable amounts (15-20% each) across this same region. Average O_3 and PV profiles were determined for each of the dominant air mass types, and these were discusses with respect to their contribution to determining the observed chemical composition of the air masses across the Pacific.

4. Acknowledgments

The authors thank Ben Barker, Chris Edwards, Shlomo Fastig, Dave Harper, Lorraine Heilman, George Insley, George Lockard, Leroy Matthews, Bill McCabe, Tony Notari, Loyd Overbay, Larry Petway, Jerry Williams, at the NASA Langley Research Center (LaRC) for their assistance in all aspects related to installing, operating, and maintaining the airborne UV DIAL and LASE systems on the DC-8 during the PEM Tropics B field experiment and in post mission data reduction and analyses tasks. The MTP work performed by MJM was carried out by the Jet Propulsion Laboratory, California Institute of Technology, under a contract with NASA. We appreciate the cooperation of the NASA Dryden Flight Research Center's DC-8 flight crew in conducting this field experiment. The funding for this investigation came from the NASA Tropospheric Chemistry Program.

5. References

Browell, E. V., Remote sensing of tropospheric gases and aerosols with an airborne DIAL system, in Optical Laser Remote Sensing, edited by D. K. Killinger and A. Mooradian, pp. 138-147, Springer-Verlag, New York, 1983.

Browell, E. V., Differential absorption lidar sensing of ozone, Proc. IEEE, 77, 419-432, 1989.

Browell, E., and S. Ismail, First lidar measurements of water vapor and aerosols from a high-altitude aircraft. Proc. OSA Optical Remote Sensing of the Atmosphere, Salt Lake City, Utah, , OSA Technical Digest 2, pp. 212-214, February 5-9, 1995.

Browell, E. V., A. F. Carter, S. T. Shipley, R. J. Allen, C. F. Butler, M. N. Mayo, J. H. Siviter, Jr., and W. M. Hall, NASA multipurpose airborne DIAL system and measurements of ozone and aerosol profiles, Appl. Opt., 22, 522-534, 1983.

Browell, E. V. , S. Ismail, and S. T. Shipley, Ultraviolet DIAL measurements of O_3 profiles in regions of spatially inhomogeneous aerosols, Appl. Opt., 24, 2827-2836, 1985.

Browell, E. V., M. A. Fenn, C. F. Butler, W. B. Grant, J. T. Merrill, R. E. Newell, J. D. Bradshaw, S. T. Sandholm, B. E. Anderson, A. R. Bandy, A. S. Bachmeier, D. R. Blake, D. D. Davis, G. L. Gregory, B. G. Heikes, Y. Kondo, S. C. Liu, F. S. Rowland, G. W. Sachse, H. B. Singh, R. W. Talbot, and D. C. Thornton, Large-scale air mass characteristics observed over the Western Pacific during summertime, J. Geophys. Res., 101, 1691-1712, 1996a.

Browell, E. V., M. A. Fenn, C. F. Butler, W. B. Grant, M. B. Clayton, J. Fishman, A. S. Bachmeier, B. E. Anderson, G. L. Gregory, H. E. Fuelberg, J. D. Bradshaw, S. T. Sandholm, D. R. Blake, B. G. Heikes, G. W. Sachse, H. B. Singh, and R. W. Talbot, Ozone and aerosol

distributions and air mass characteristics over the South Atlantic Basin during the burning season, J. Geophys. Res., 101, 24,043-24,068, 1996b.

Browell, E. V., S. Ismail, W. M. Hall, A. S. Moore, Jr., S. A. Kooi, V. G. Brackett, M. B. Clayton, J. D. W. Barrick, F. J. Schmidlin, N. S. Higdon, S. H. Melfi, and D. N. Whiteman, LASE validation experiment, in Advances in Atmospheric Remote Sensing with Lidar, A. Ansmann, R. Neuber, P. Rairoux, and U. Wandinger, eds., pp. 289-295, Springer Verlag, New York, 1997.

Browell, E. V., S. Ismail, W. B. Grant, Differential Absorption Lidar (DIAL) measurements from air and space, Appl. Phys.-B, 67, 399-410, 1998.

Browell, E. V., S. Ismail, and R. Ferrare, Hurricane water vapor, aerosol, and cloud distributions determined from airborne lidar measurements, Proc. AMS Symp. on Lidar Atmos. Monitoring, Long Beach, California, 65-67, January 9-14, 2000.

Fenn, M. A., E. V. Browell, and C. F. Butler, Airborne lidar measurements of ozone and aerosols during PEM-West A and PEM-West B, in Advances in Atmospheric Remote Sensing with Lidar, A. Ansmann, R. Neuber, P. Rairoux, and U. Wandinger, eds., pp. 355-358, Springer Verlag, New York, 1996.

Fenn, M. A., E. V. Browell, C. F. Butler, W. B. Grant, S. A. Kooi, M. B. Clayton, et al., Ozone and aerosol distributions and air mass characteristics over the south Pacific during the burning season, J. Geophys. Res., 104, 16,197-16,212, 1999.

Ferrare, R., E. V. Browell, S. Ismail, W. Smith, W. Edwards, et al., LASE measurements of water vapor, aerosols, and clouds during CAMEX-3, Proc. 1999 OSA Symposium on Optical Remote Sensing of the Atmosphere, 114-116, 1999.

Ferrare, R., S. Ismail, E. Browell, V. Brackett, M. Clayton, S. Kooi, S. H. Melfi, D. Whiteman, G. Schwemmer, K. Evans, P. Russell, J. Livingston, B. Schmid, B. Holben, L. Remer, A. Smirnov, and P. V. Hobbs, Comparison of aerosol optical properties and water vapor among ground and airborne lidars and Sun photometers during TARFOX, J. Geophys. Res., 105, 9917-9933, 2000a.

Ferrare, R. A. , S. Ismail, E. V. Browell, V. G. Brackett, S. A. Kooi, M. B. Clayton, P. V. Hobbs, S. Hartley, J. P. Veefkind, P. B. Russell, J. Livingston, D. Tanre, and P. Hignett, Comparisons of LASE, aircraft, and satellite measurements of aerosol optical properties and water vapor during TARFOX, J. Geophys. Res., 105, 9935-9947, 2000b.

Fishman, J., V. G. Brackett, E. V. Browell, and W. B. Grant, Tropospheric ozone derived from TOMS/SBUV measurements during TRACE A, J. Geophys. Res., 101, 24,069-24,082, 1996.

Fuelberg, H. E., R. E. Newell, S. P. Longmore, Y. Zhu, D. J. Westberg, E. V. Browell, et al., A meteorological overview of the Pacific Exploratory Mission (PEM) Tropics period, J. Geophys. Res., 104, 5585-5622, 1999.

Fuelberg et al., A meteorological overview of the PEM Tropics B mission, J. Geophys. Res., this issue, 2000.

Hoell , J. M.., D. D. Davis, D. J. Jacob, M. O. Rodgers, R. E. Newell, H. E. Fuelberg, r. J. McNeal, J. L. Raper, and R. J. Bendura, Pacific Exploratory Mission in the tropical Pacific: PEM-Tropics A, August-September 1996, J. Geophys. Res., 104, 5567-5583, 1999.

Jacob/Davis et al., PEM Tropics B overview paper, J. Geophys. Res., this issue, 2000.

Moore, A. S., Jr., K. E. Brown, W. M. Hall, J. C. Barnes, W. C. Edwards, L. B. Petway, A. D. Little, W. S. Luck, Jr., I. W. Jones, C. W. Antill, Jr., E. V. Browell, and S. Ismail, Development of the Lidar Atmospheric Sensing Experiment (LASE) -- An advanced

airborne DIAL instrument, in Advances in Atmospheric Remote Sensing with Lidar, A. Ansmann, R. Neuber, P. Rairoux, and U. Wandinger, eds., pp. 281-288, Springer Verlag, New York, 1997.

Richter, D. A., E. V. Browell, C. F. Butler, and N. S. Higdon, Advanced airborne UV DIAL system for stratospheric and tropospheric ozone and aerosol measurements, in Advances in Atmospheric Remote Sensing with Lidar, A. Ansmann, R. Neuber, P. Rairoux, and U. Wandinger, eds., pp. 395-398, Springer Verlag, New York, 1997.

Schultz, M. G., D. J. Jacob, Y. Wang, J. A. Logan, E. L. Atlas, D. R. Blake, N. J. Blake, J. D. Bradshaw, E. V. Browell, et al., On the origin of tropospheric ozone and NOx over the tropical South Pacific, J. Geophys. Res., 104, 5829-5843, 1999.

Singh, H. B., W. Viezee, Y. Chen, J. Bradshaw, s. Sandholm, D. Blake, N. Blake, b. Heikes, J. Snow, R. Talbot, E. Browell, G. Gregory, G. Sachse, and S. Vay, Biomass burning influences on the composition of the remote South Pacific troposphere: Analysis based on observations from PEM-Tropics-A, Atmos. Env., 34, 635-644, 2000.

Talbot, R. W., J. E. Dibb, E. M. Scheuer, D. R. Blake, N. J. Blake, G. L. Gregory, G. W. Sachse, J. D. Bradshaw, S. T. Sandholm, and H. B. Singh, Influence of biomass combustion emissions on the distribution of acidic trace gases over the southern Pacific basin during austral springtime, J. Geophys. Res., 104, 5623-5634, 1999.

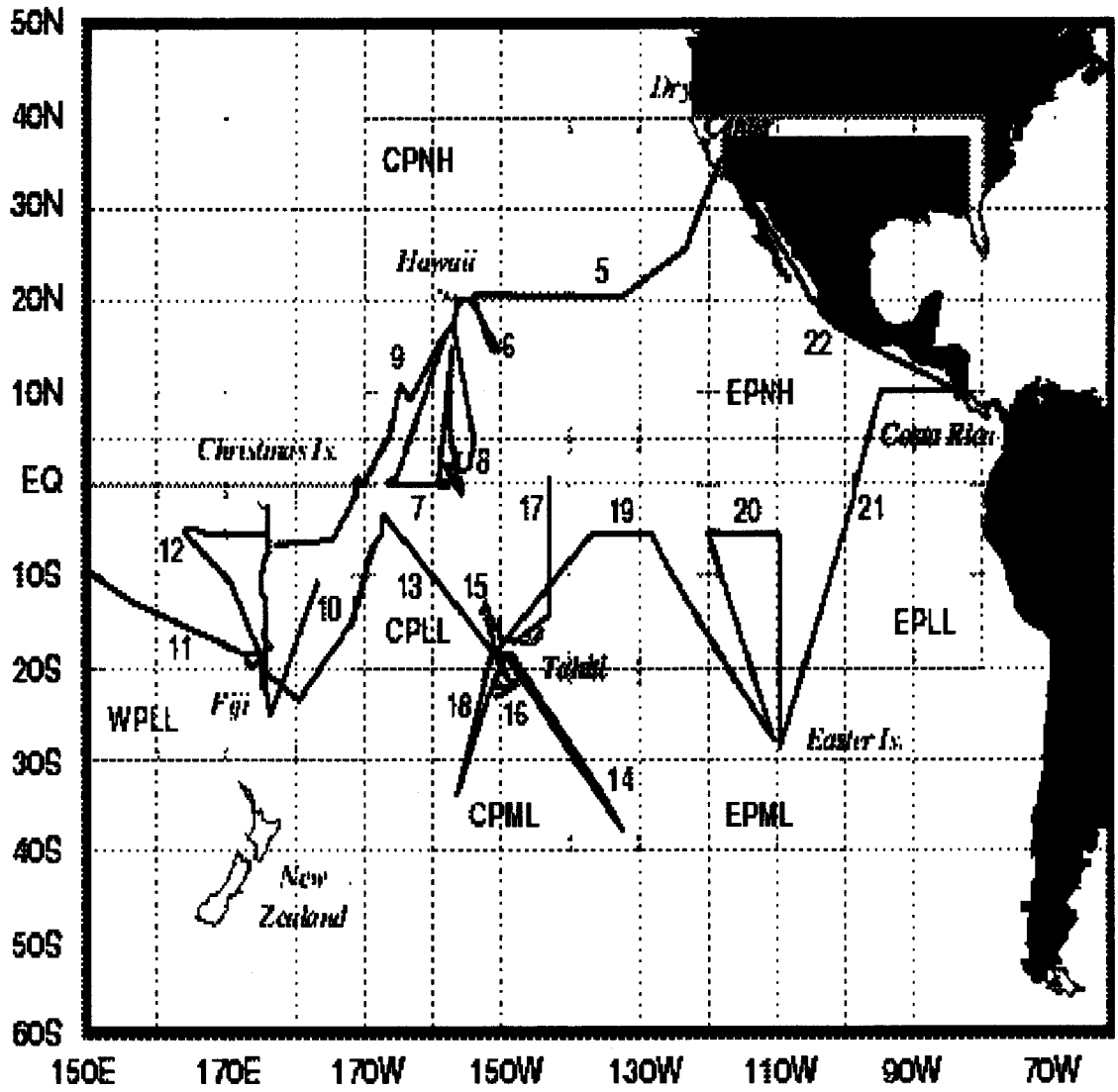

Figure 1. Map of PEM-Tropics B DC-8 flight tracks from 19 February to 18 April 1999 with flight numbers marked and regions used in air mass characterization investigations: Central Pacific Northern Hemisphere (CPNH), Eastern Pacific Northern Hemisphere (EPNH), Western Pacific Low Latitude (WPLL), Central Pacific Low Latitude (CPLL), Eastern Pacific Low Latitude (EPLL), Central Pacific Mid Latitude (CPML), and Eastern Pacific Mid Latitude (EPML).

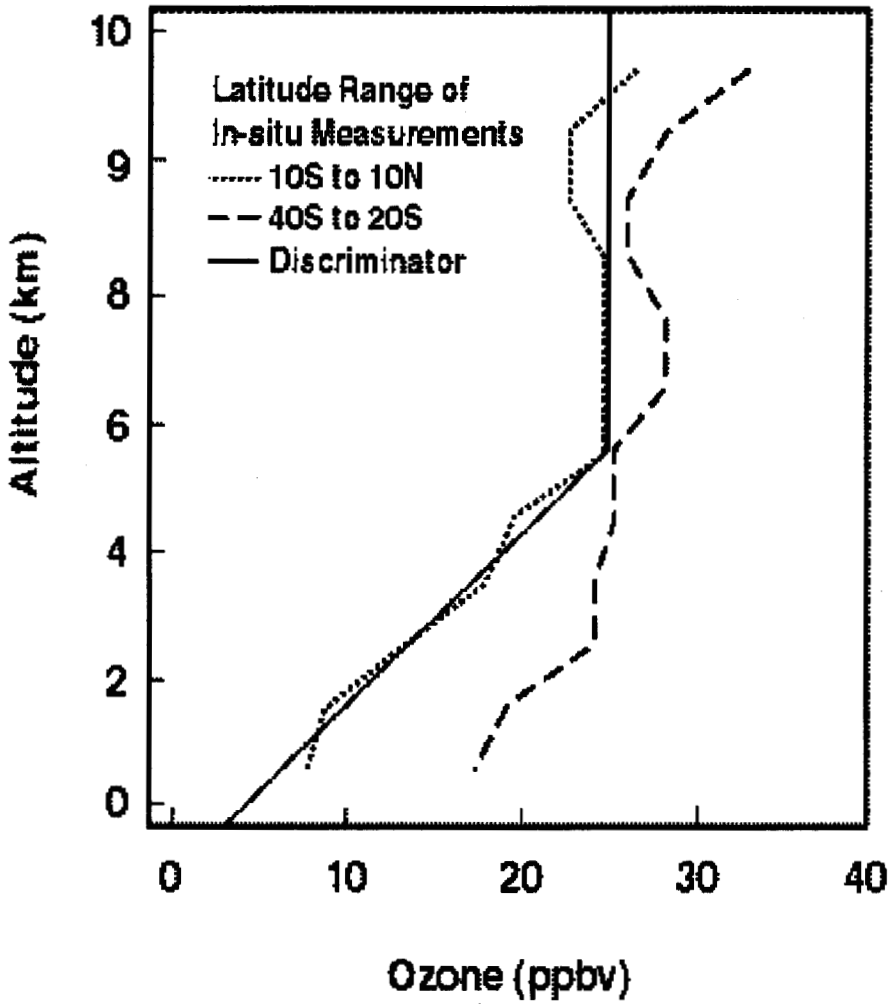

Figure 2. Average in situ ozone profiles measured over mid-Pacific during PEM-Tropics B in the low (10°S to 10°N) and mid (40°S to 20°S) latitude ranges. Ozone profile used as the discriminator in the air mass characterization investigation is also shown.

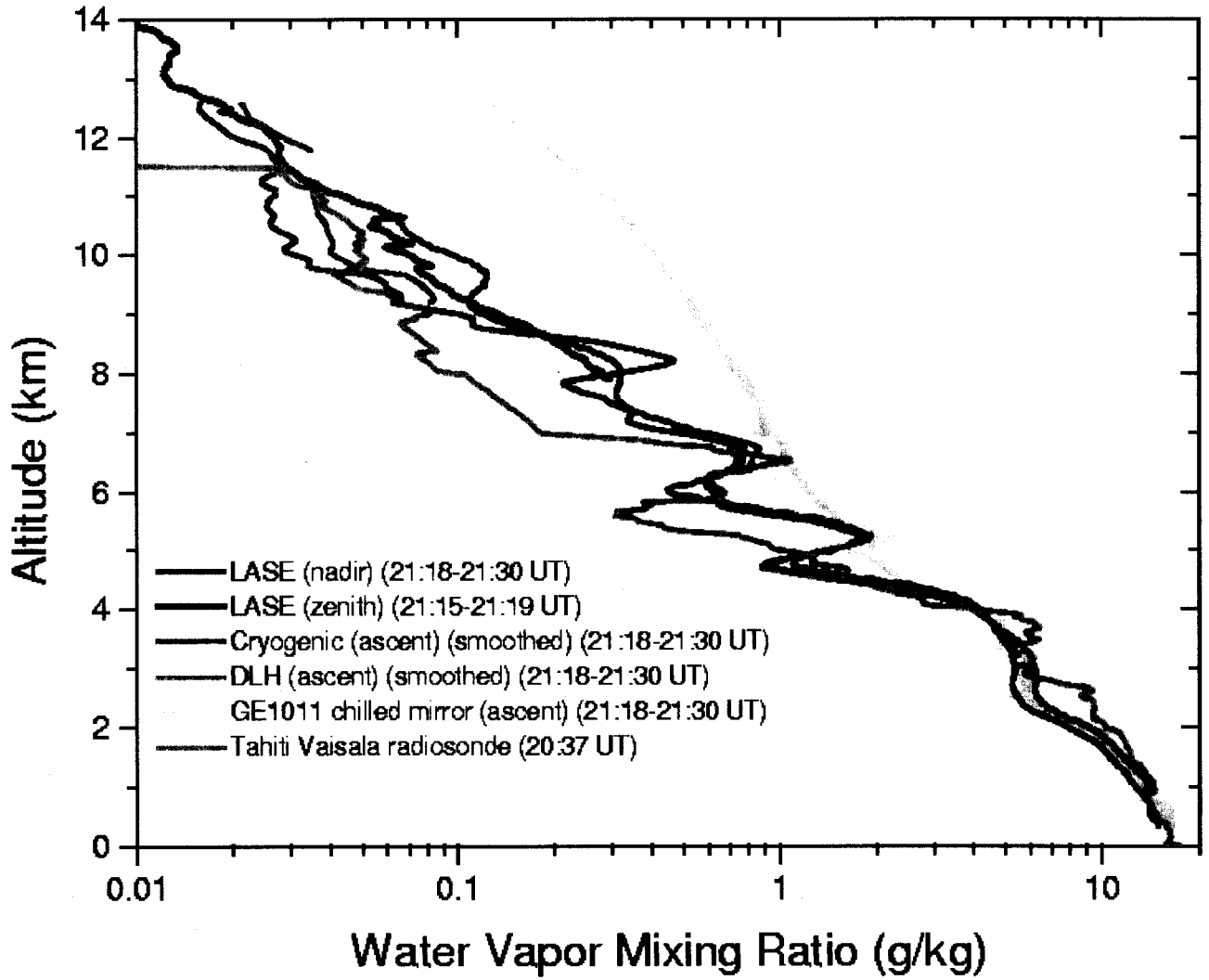

Plate 1. Water vapor profile comparisons between LASE nadir and zenith remote measurements and in situ measurements of the Cryogenic Hygrometer, Diode Laser Hygrometer (DLH), and GE-1011 chilled mirror hygrometer on the DC-8 and the Tahiti Vaisala radiosonde on local flight from Tahiti on 2 April 1999 (Flight 15).

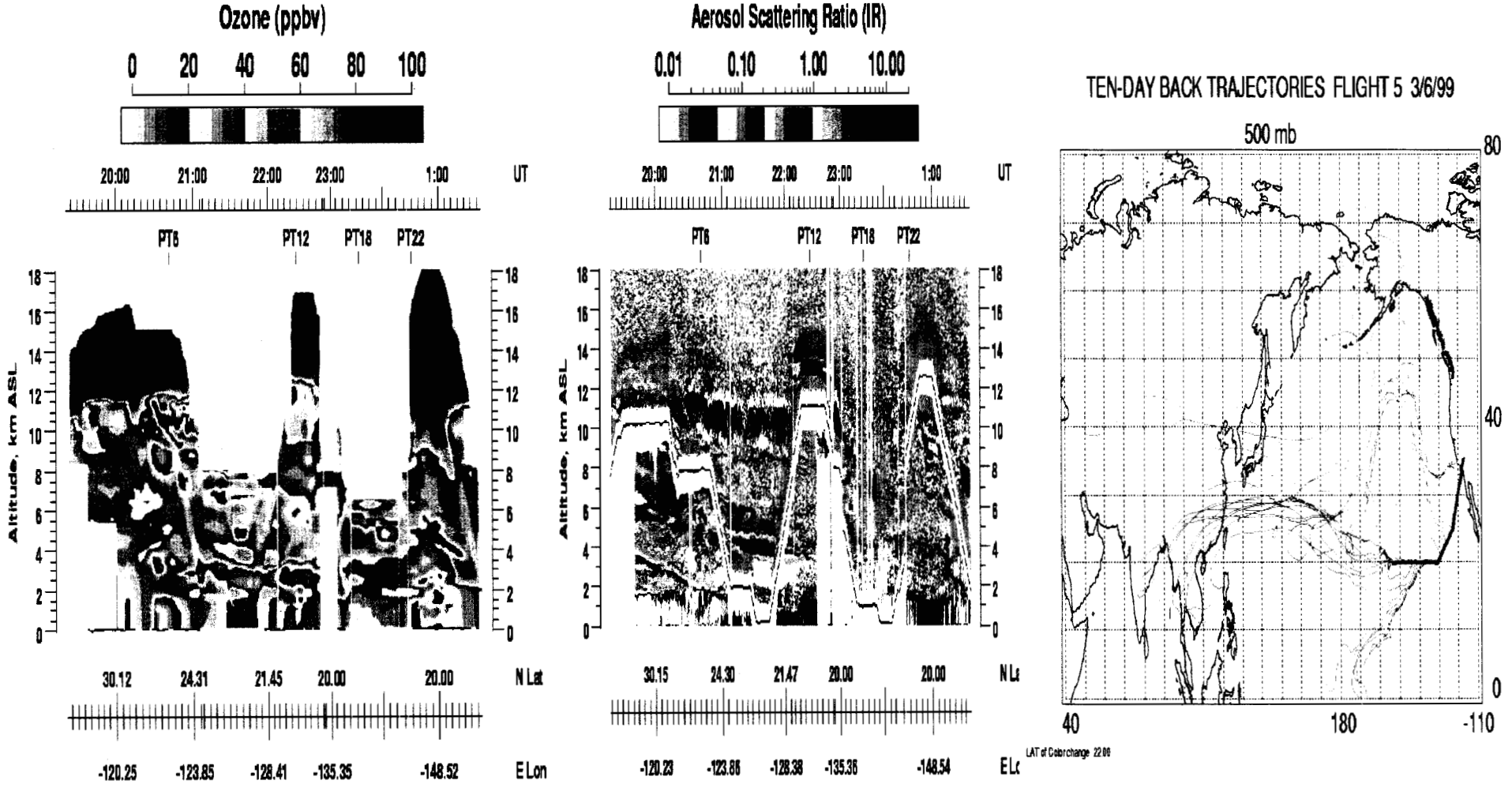

Plate 2. Ozone and aerosol scattering ratio distributions observed on flight from California to Hawaii on 6-7 March 1999 (Flight 5). The time (UT), north latitude (N Lat), and east longitude (E Lon) of the measurements are shown. Ten-day back trajectory analyses starting along the flight track at 500 mb is also shown.

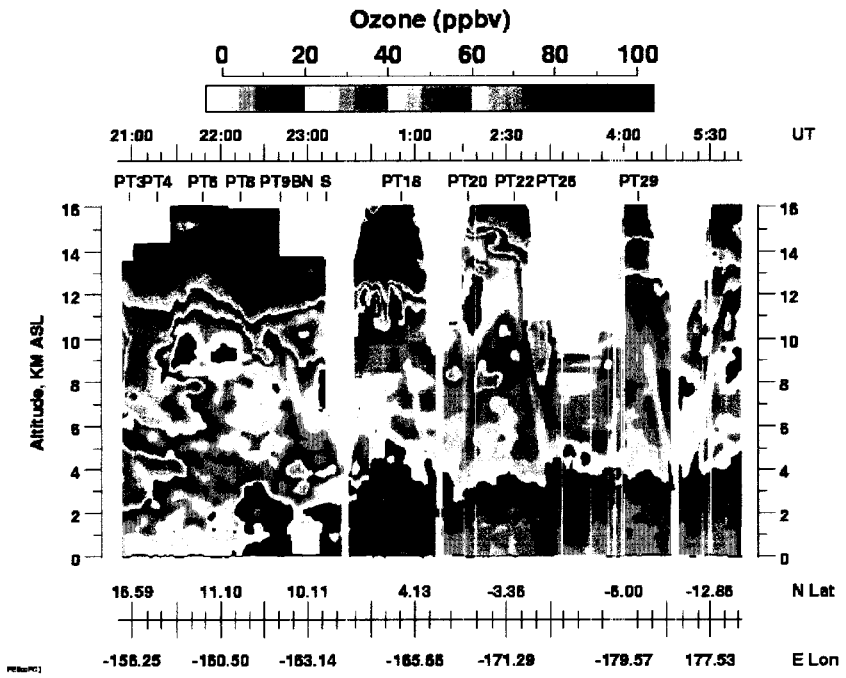

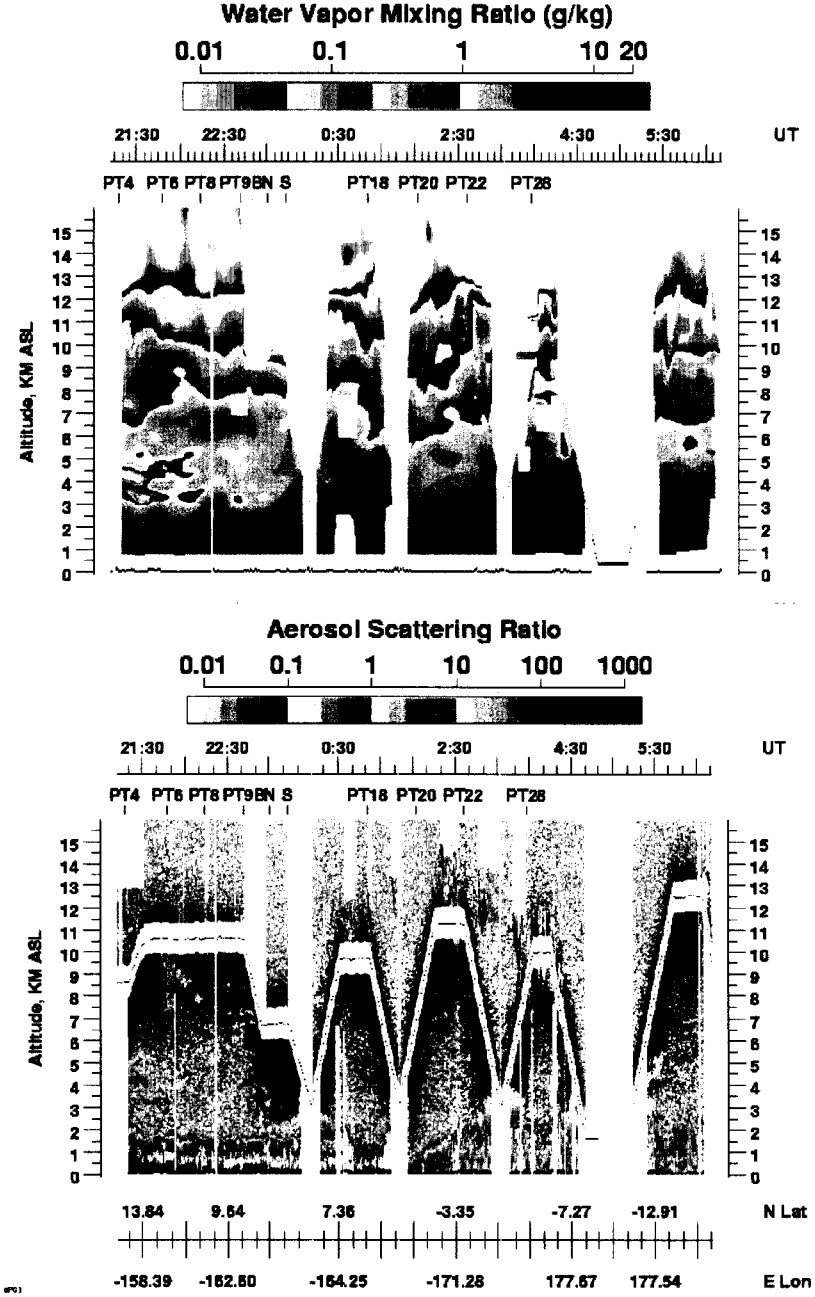

Plate 3. Ozone, H_2O, and aerosol scattering ratio distributions observed across the ITCZ on flight from Hawaii to Fiji on 17-18 March 1999 (Flight 9).

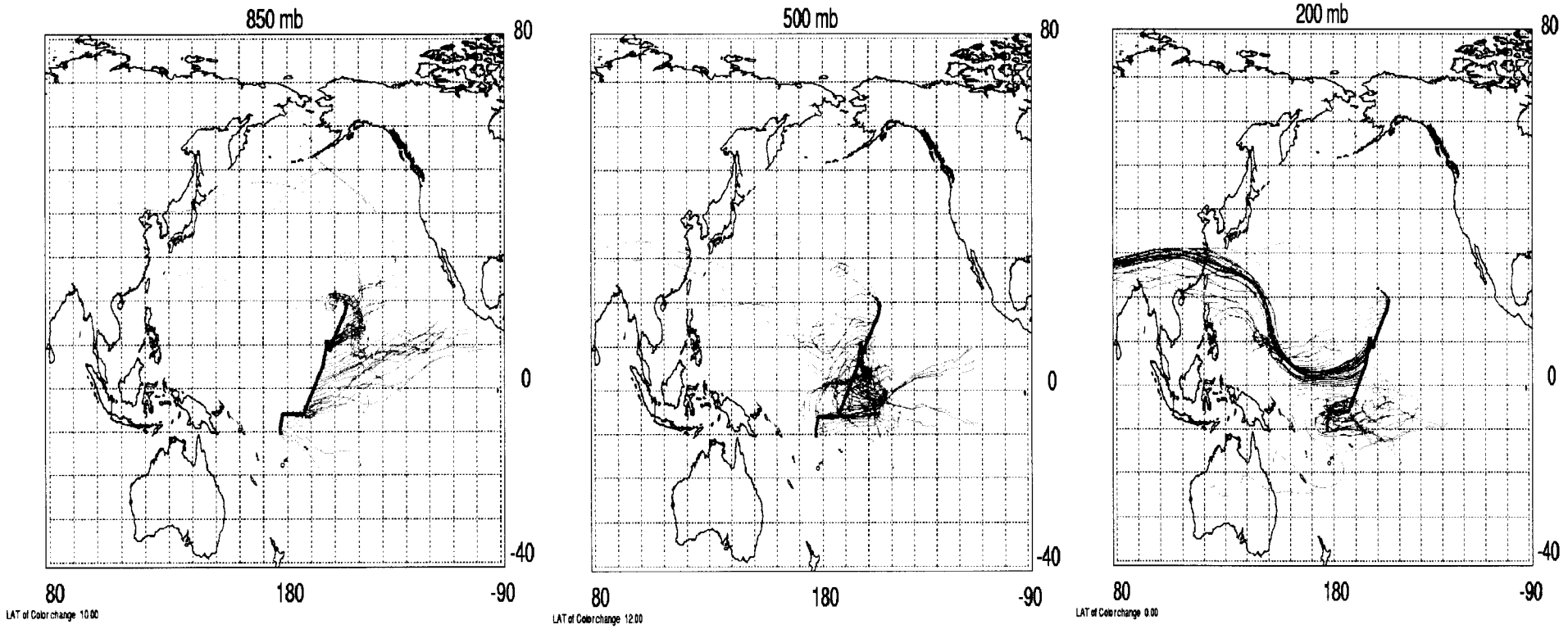

Plate 4. Ten-day back trajectory analyses starting at 200, 500, and 850 mb levels along flight track corresponding to measurements shown in Plate 3. Different colors are used to accentuate the differences in the back trajectories on either side of the ITCZ at about 10°N.

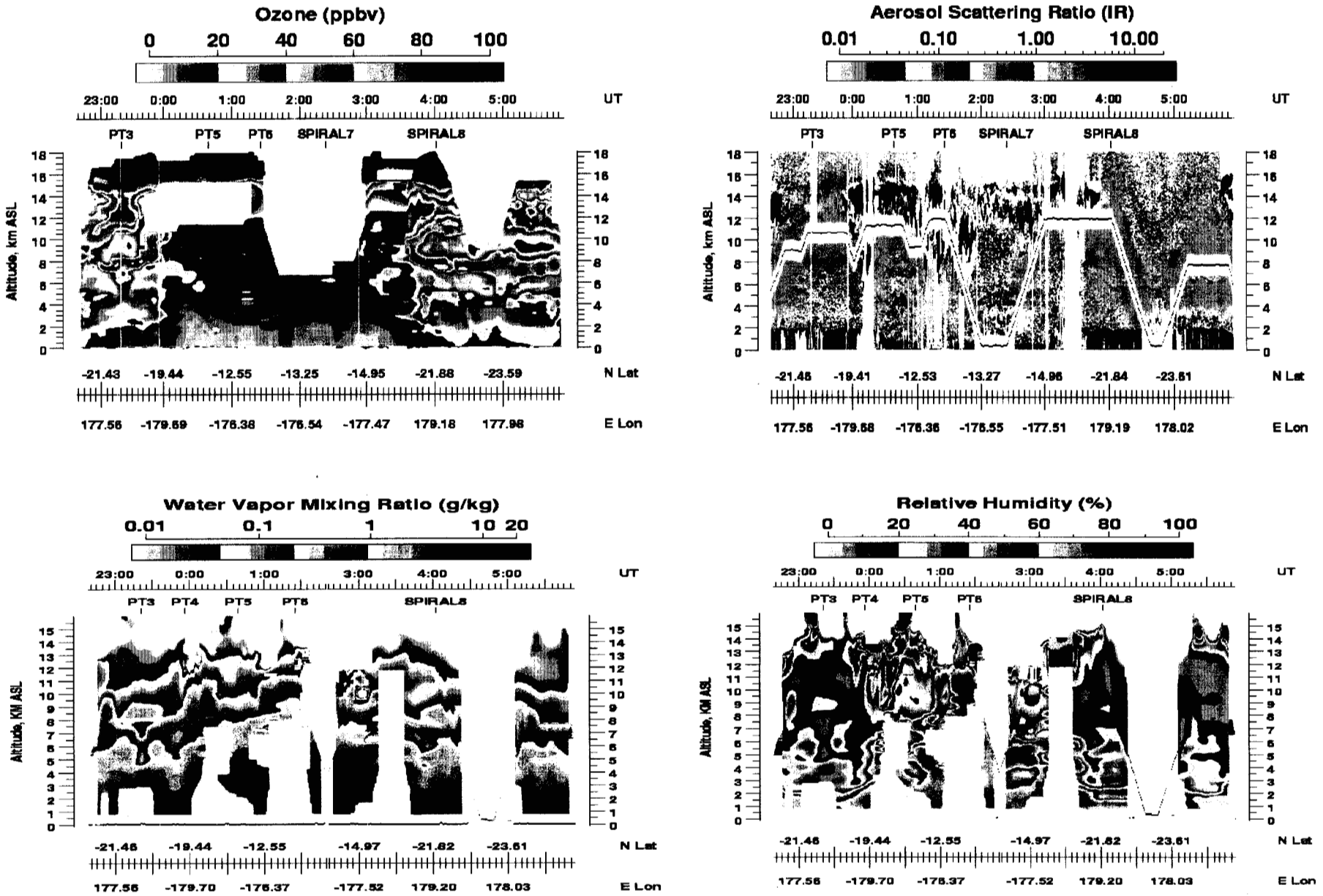

Plate 5. Ozone, aerosols, H_2O and relative humidity distributions observed across SPCZ on local flight from Fiji on 20 March 1999 (Flight 10).

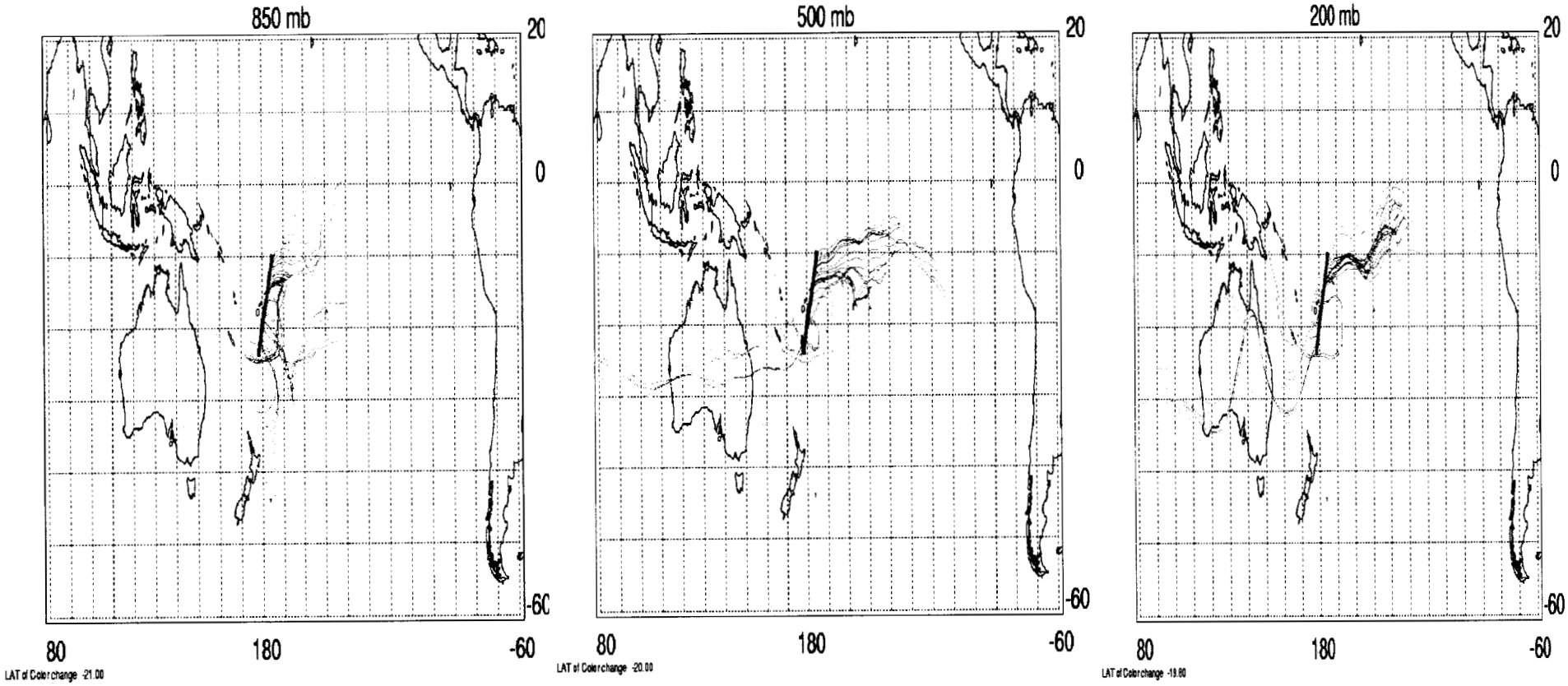

Plate 6. Ten-day back trajectory analyses starting at 200, 500, and 850 mb levels along flight track corresponding to measurements shown in Plate 5. Different colors are used to accentuate the differences in the back trajectories on either side of the SPCZ.

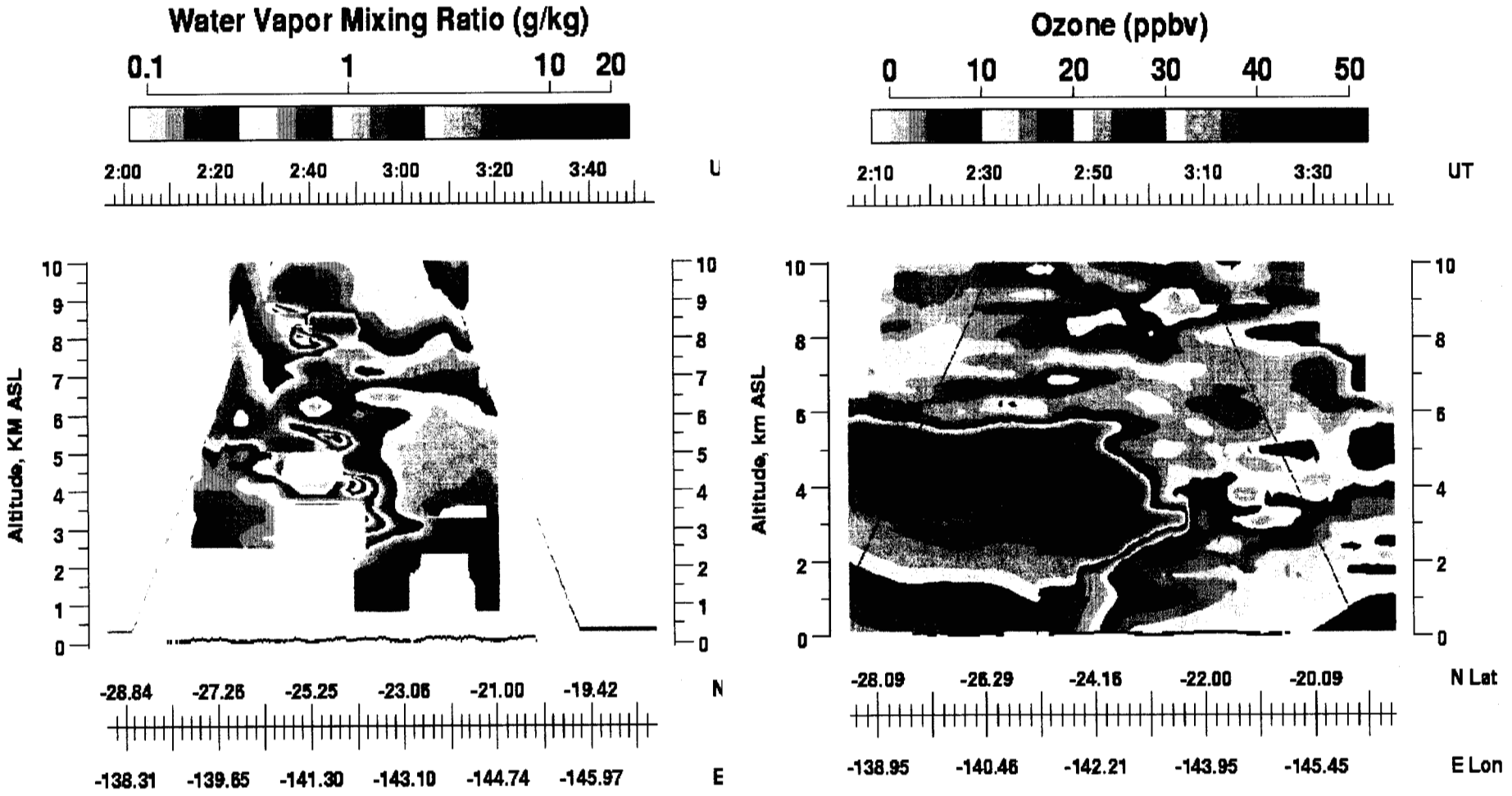

Plate 7. Water vapor and O_3 distribution across SPCZ on local flight from Tahiti on 31 March 1999 (Flight 14).

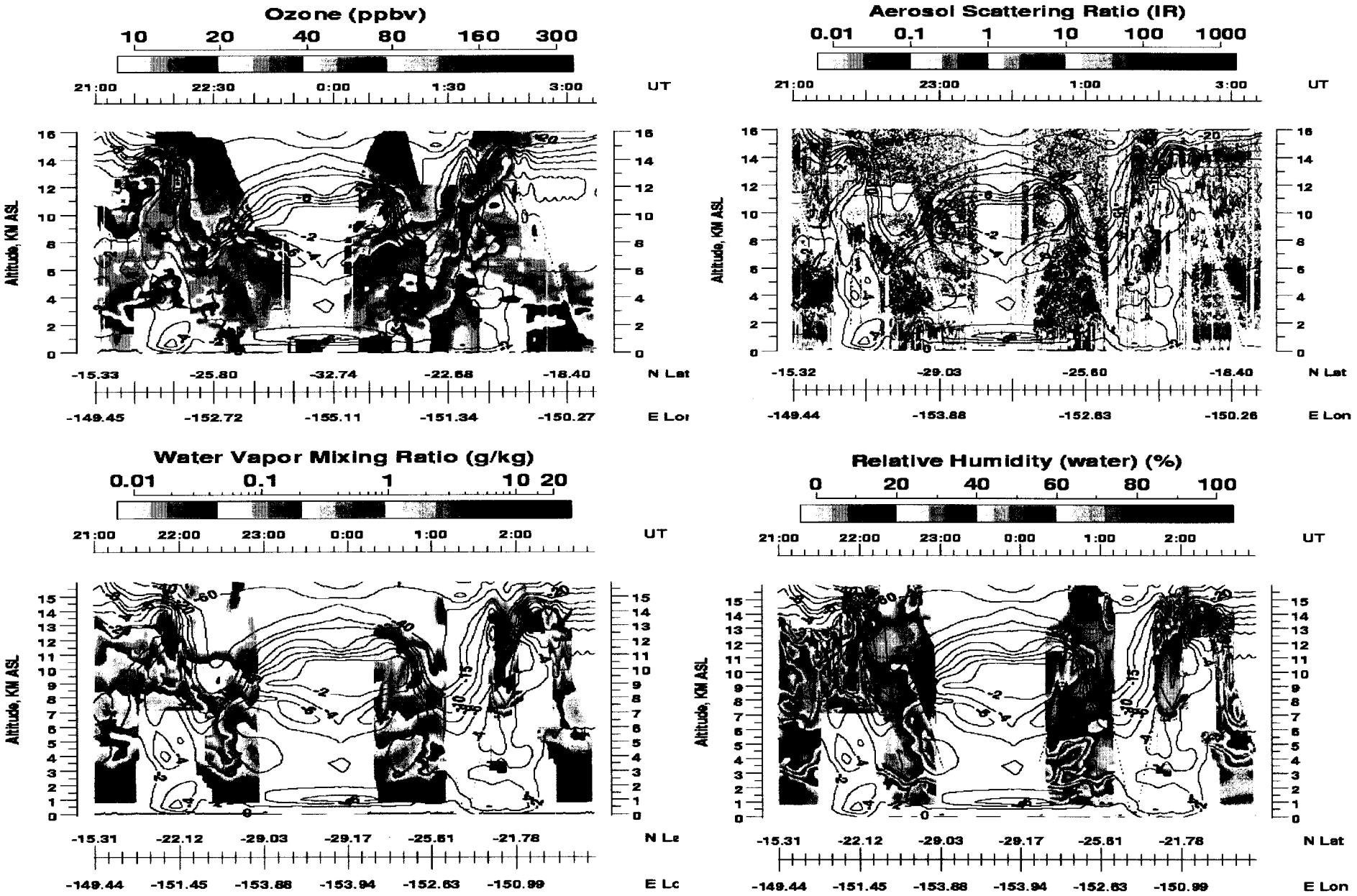

Plate 8. Ozone, aerosols, H_2O, and relative humidity observed across a front and in the vicinity of a stratospheric intrusion on local flight from Tahiti on 10-11 April 1999 (Flight 18). Isopleths of potential vorticity (PV) in units of 10^{-7} deg K m^2 kg^{-1} s^{-1} are overplotted on each distribution for comparison.

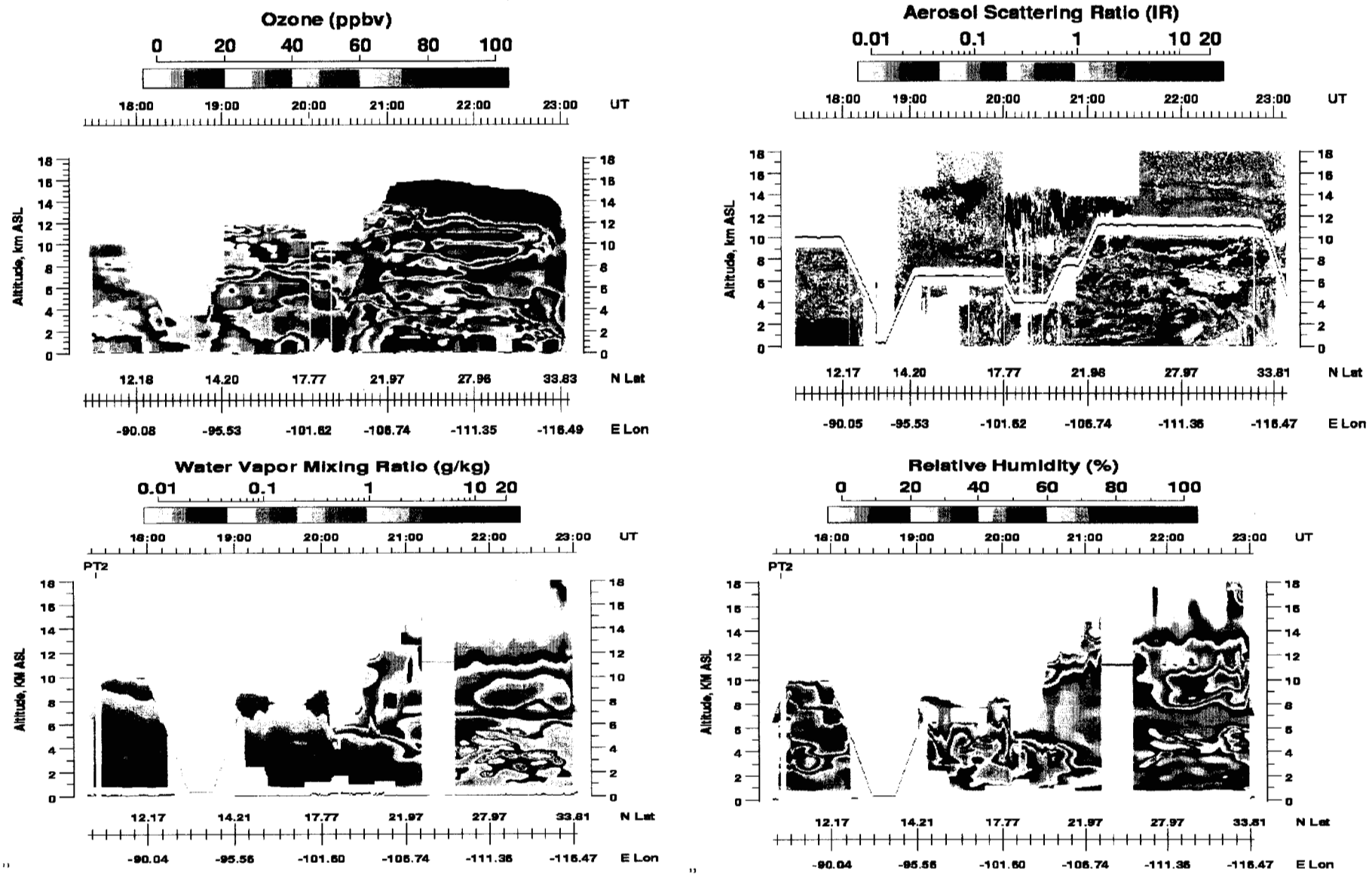

Plate 9. Ozone, aerosols, H_2O, and relative humidity observed across different air masses on survey flight from Costa Rica to California on 18 April 1999 (Flight 22).

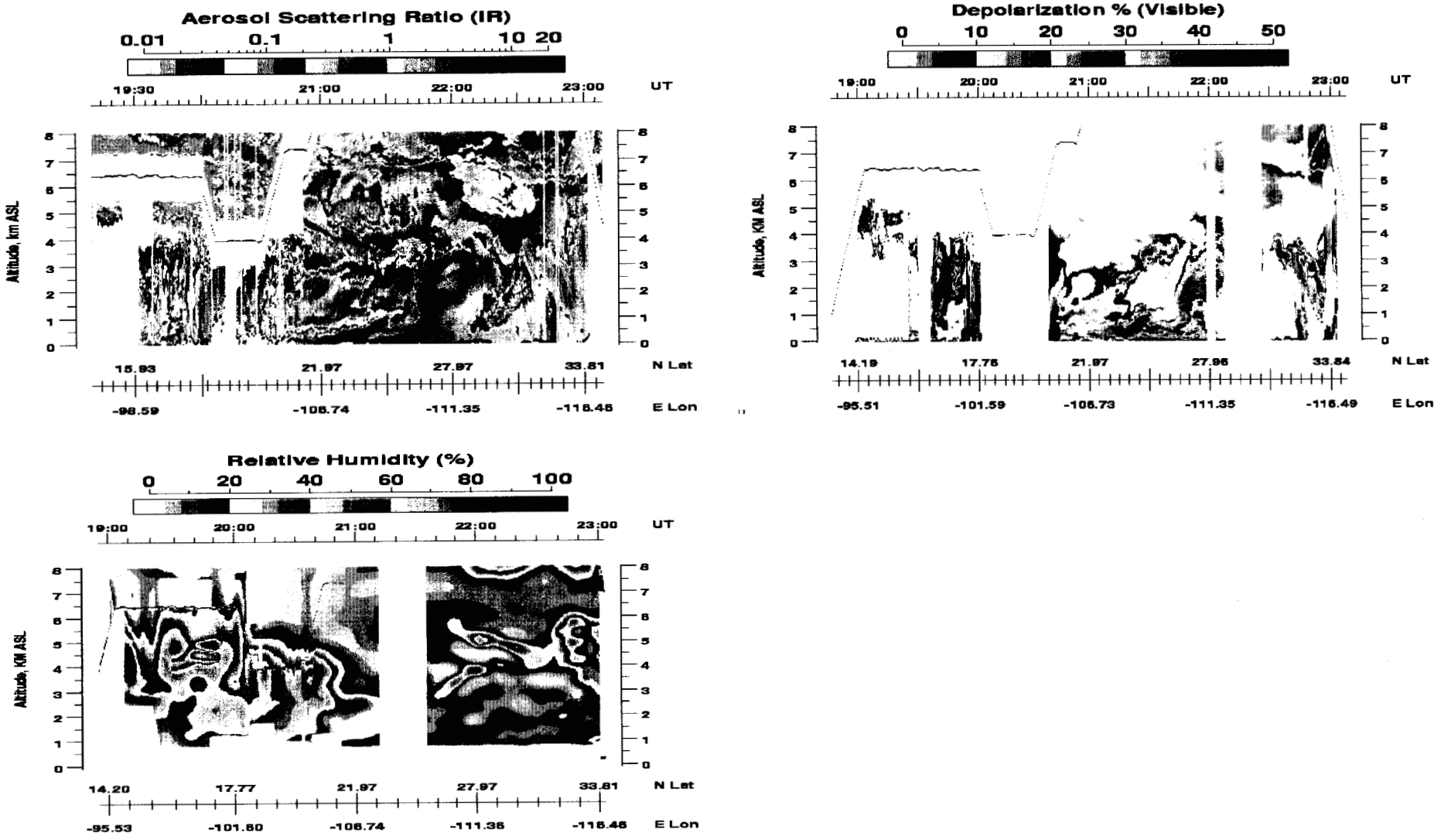

Plate 10. Aerosol scattering ratio, aerosol depolarization, and relative humidity for the same flight shown in Plate 9.

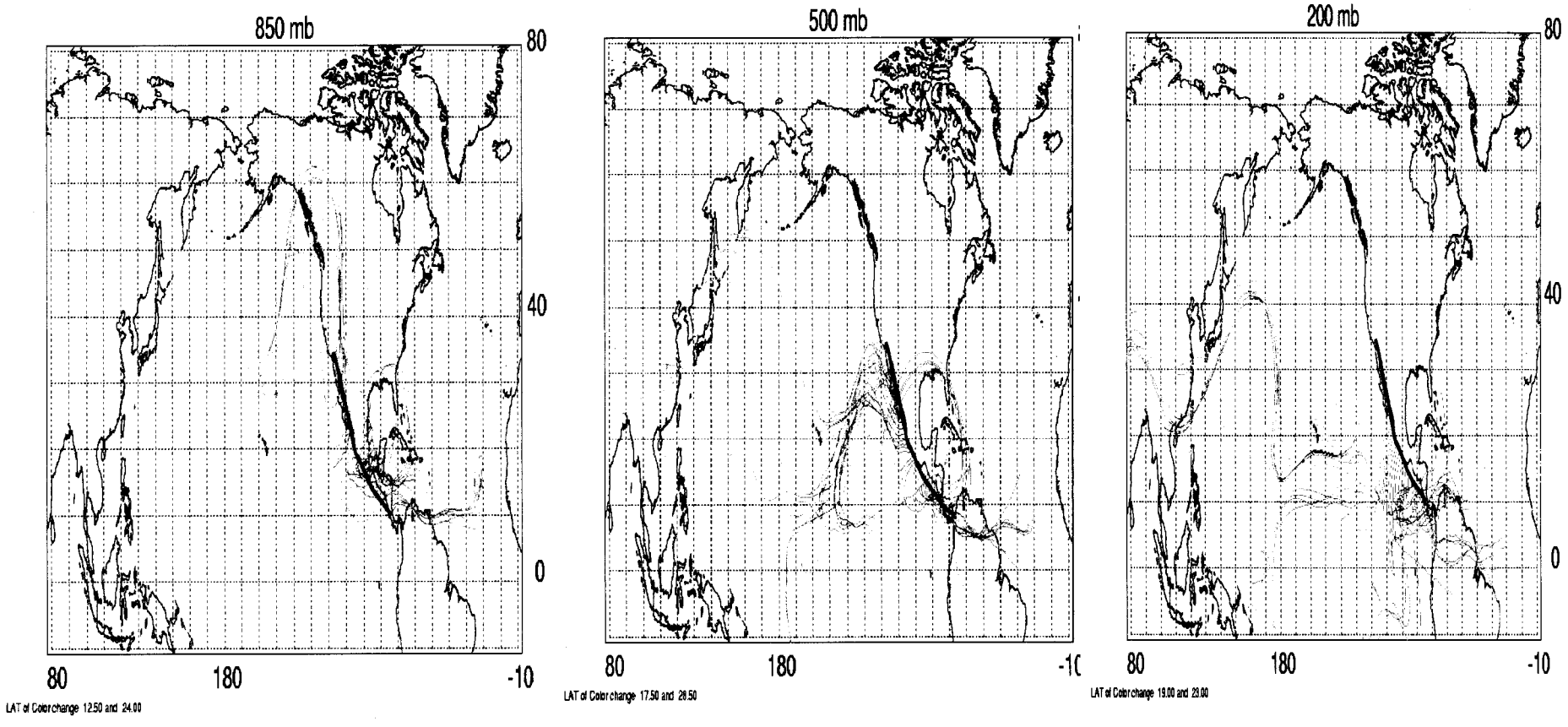

Plate 11. Ten-day backtrajectories shown at 850 mb along flight track from Costa Rica to California on 18 April 1999 (see measurements shown in Plates 9 and 10). Different colors are used to show the back trajectories for three regions having distinctly different air mass histories along the flight track.

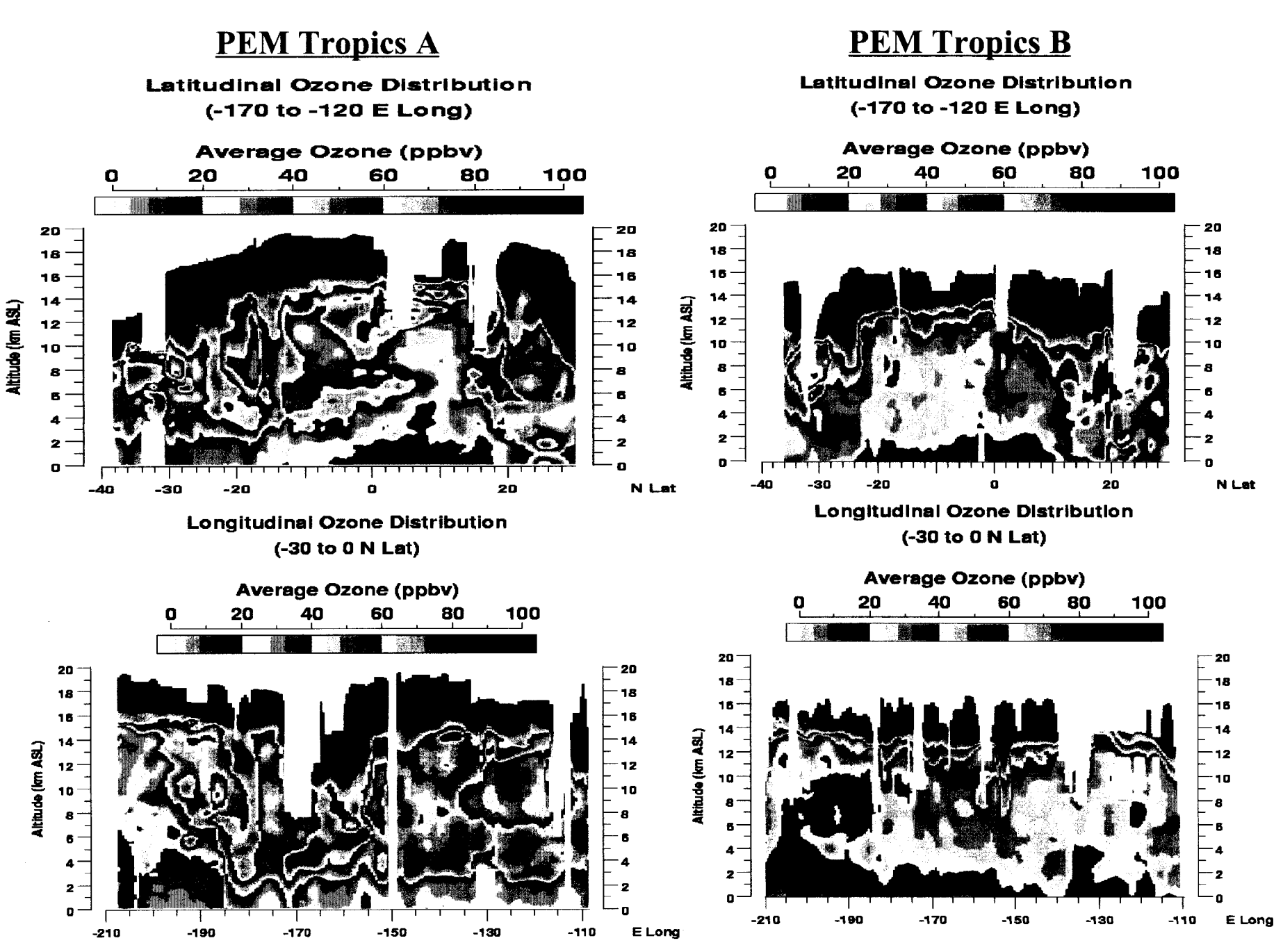

Plate 12. Comparison of average latitudinal and longitudinal O_3 cross sections observed during PEM Tropics A and B.

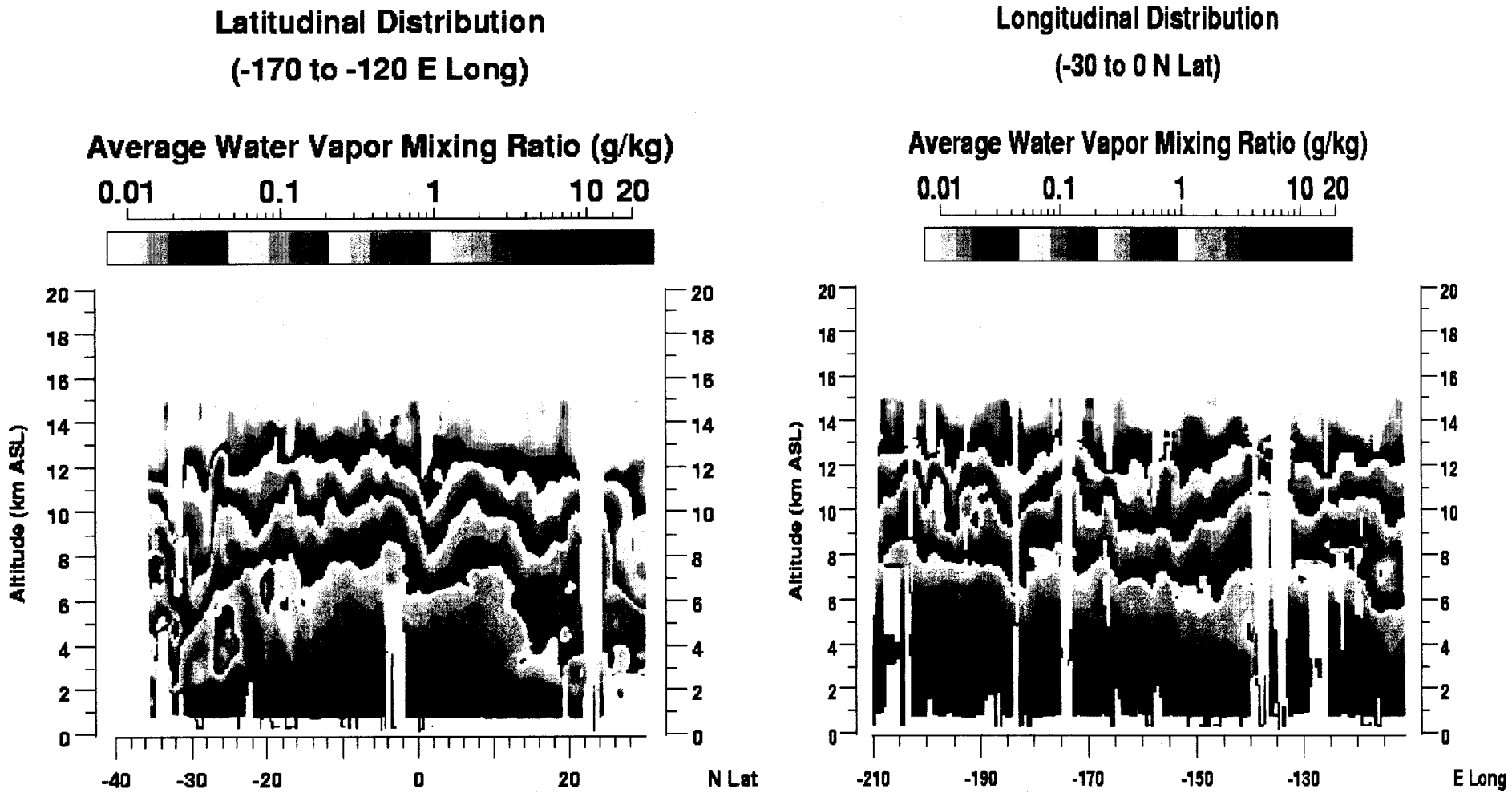

Plate 13. Average latitudinal and longitudinal H_2O distribution observed during PEM Tropics B.

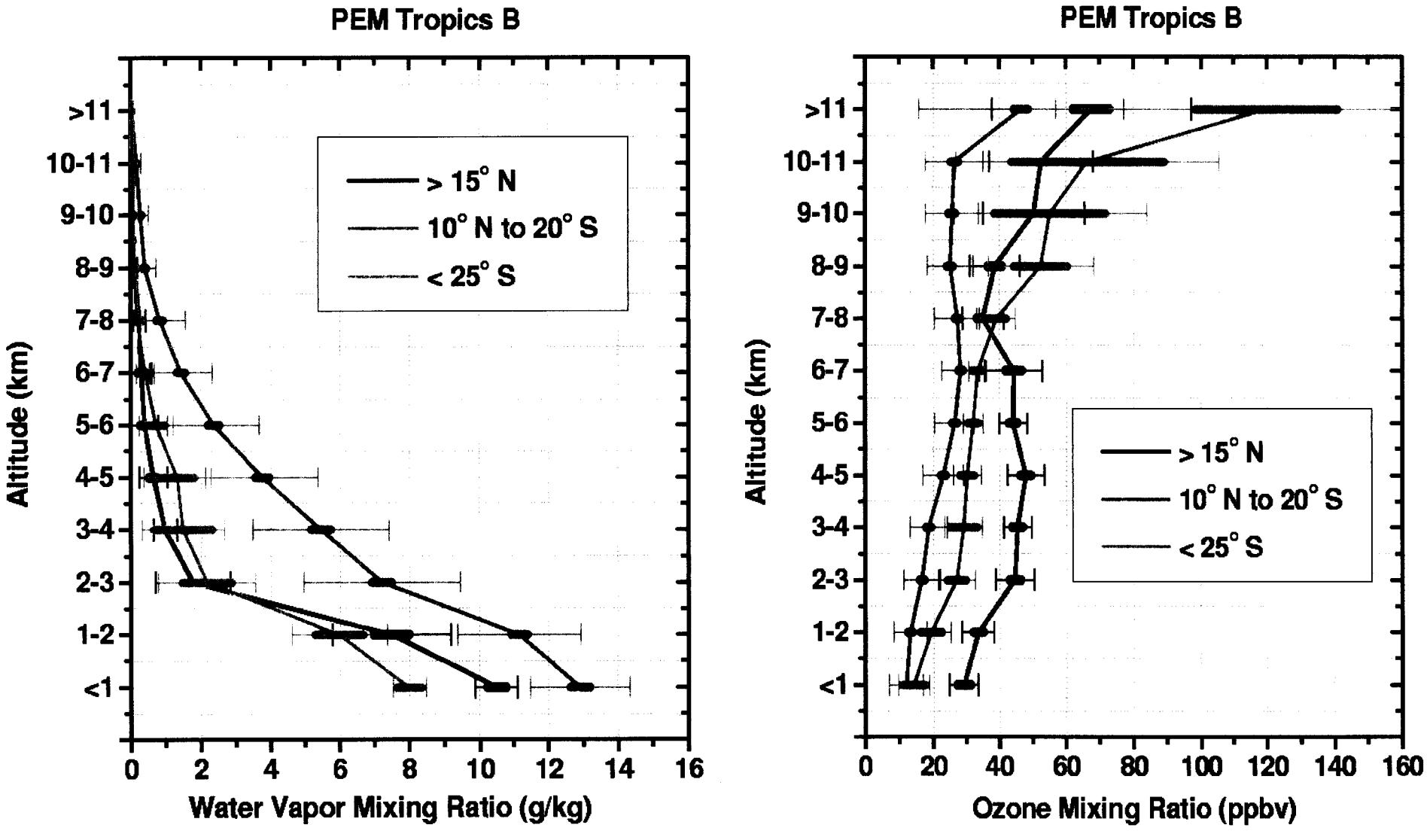

Plate 14. Average H_2O and O_3 profiles observed generally north of ITCZ (>15°N), between the ITCZ and SPCZ (10°N to 20°S), and south of the SPCZ (<25°S) on Flights 6-18.

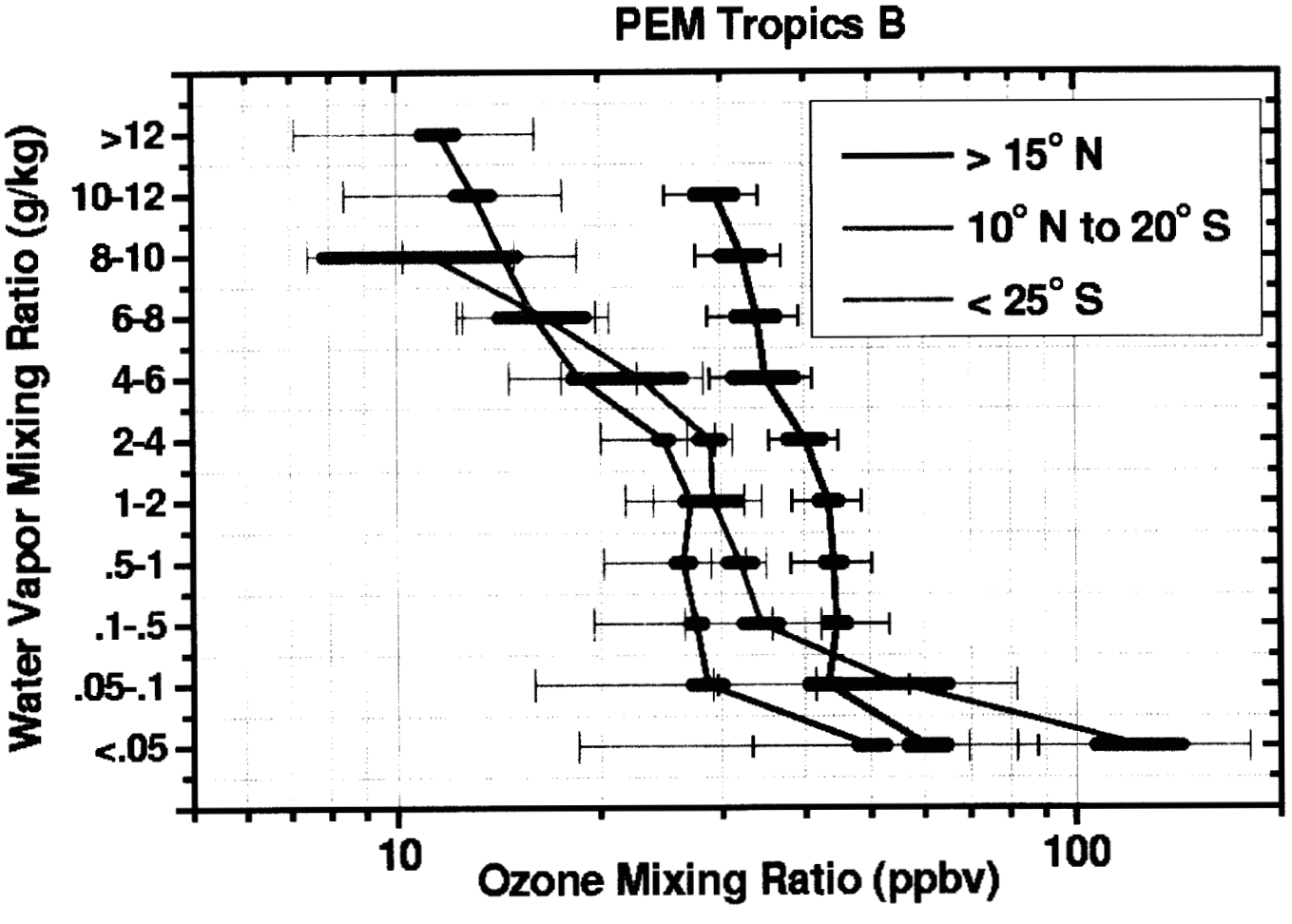

Plate 15. Average H_2O/O_3 correlations in the different domains defined in Plate 14.

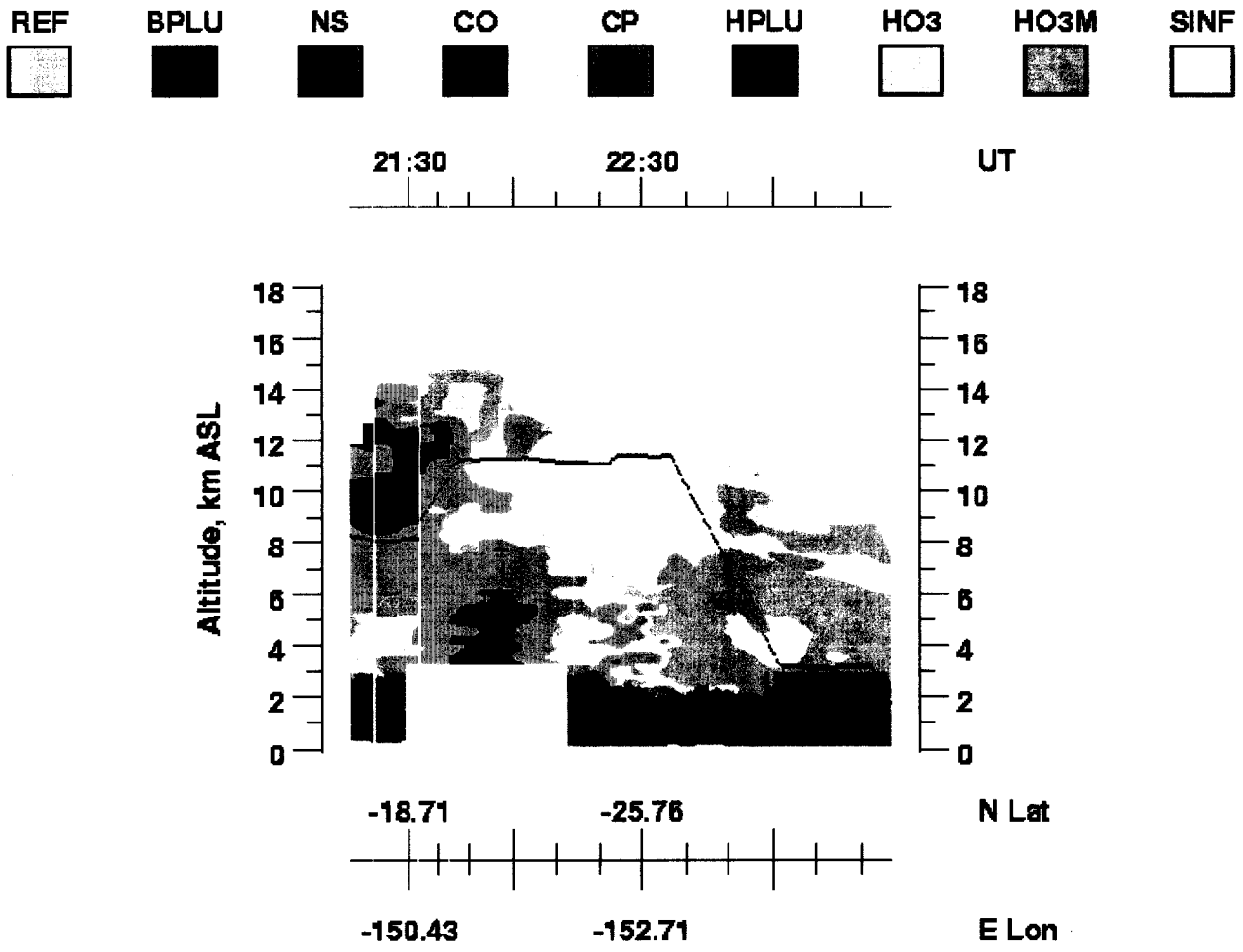

Plate 16. Example of airmass characterization based on the O_3, aerosol, and PV criteria for local Tahiti flight on 10-11 April 1999 (Flight 18). The air mass types are: Reference (REF), Background-O_3 Plume (BPLU), Near Surface (NS), Convective Outflow (CO), Clean Pacific (CP), High-O_3 Plume (HPLU), High O_3 with low PV (HO3), High O_3 with moderate PV (HO3M), and High O_3 with high PV or Stratospherically Influenced Air (SINF).

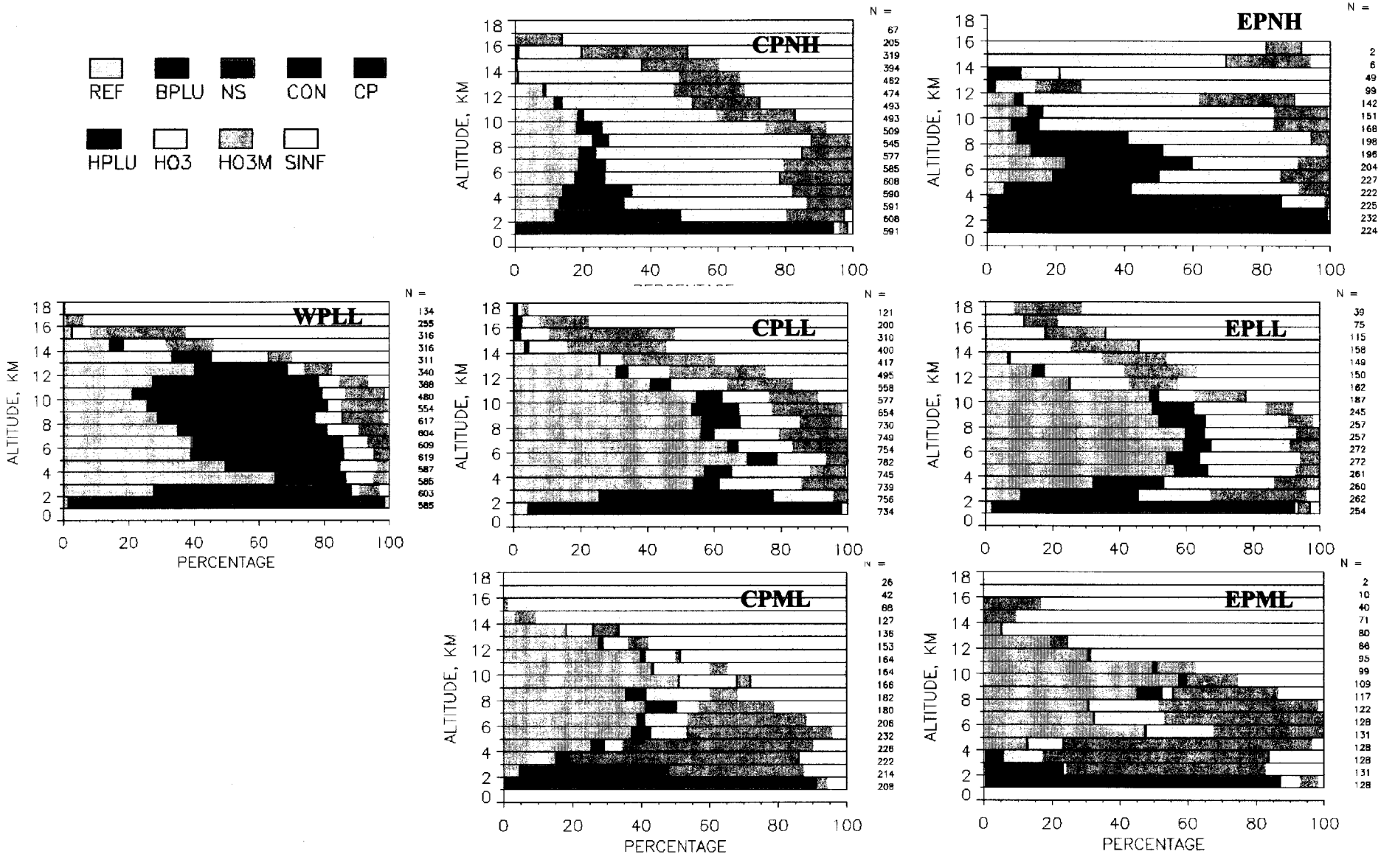

Plate 17. Percentage of time different air masses were observed at different altitudes in the various regions over the Pacific (see Figure 1).

Average Composition

Average Ozone

Average Potential Vorticity

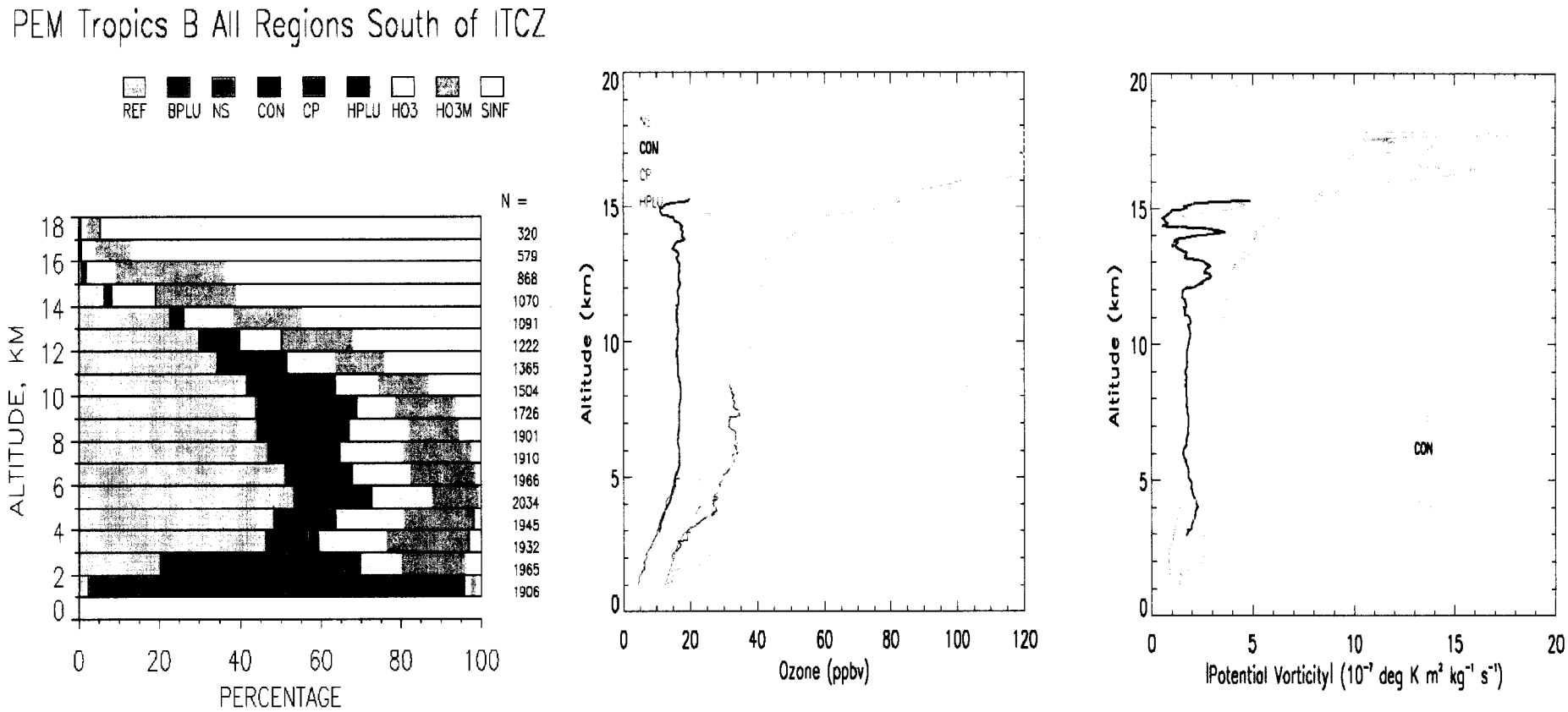

Plate 18. Average percentage of time the various air masses were observed at different altitudes south of the ITCZ and the average O_3 and PV profiles for each of the major air mass categories.